

# NAVAL POSTGRADUATE SCHOOL

## Monterey, California

AD-A257 341



DTIC  
ELECTE  
NOV 23 1992  
S C D

## THESIS

THE ATMOSPHERIC EMISSION METHOD OF  
CALCULATING THE NEUTRAL ATMOSPHERE AND  
CHARGED PARTICLE DENSITIES IN THE UPPER  
ATMOSPHERE

by

Kenneth L. McElroy Jr.

December 1992

Thesis Advisor:

David D. Cleary

Approved for public release; distribution is unlimited

92-29934



UNCLASSIFIED

SECURITY CLASSIFICATION OF THIS PAGE

REPORT DOCUMENTATION PAGE				
1a. REPORT SECURITY CLASSIFICATION			1b. RESTRICTIVE MARKINGS	
2a. SECURITY CLASSIFICATION AUTHORITY			3. DISTRIBUTION/AVAILABILITY OF REPORT	
2b. DECLASSIFICATION/DOWNGRADING SCHEDULE			Approved for public release; distribution is unlimited.	
4. PERFORMING ORGANIZATION REPORT NUMBER(S)			5. MONITORING ORGANIZATION REPORT NUMBER(S)	
6a. NAME OF PERFORMING ORGANIZATION Naval Postgraduate School	6b. OFFICE SYMBOL (If applicable) PH	7a. NAME OF MONITORING ORGANIZATION Naval Postgraduate School		
6c. ADDRESS (City, State, and ZIP Code) Monterey, CA 93943-5000		7b. ADDRESS (City, State, and ZIP Code) Monterey, CA 93943-5000		
8a. NAME OF FUNDING/SPONSORING ORGANIZATION	8b. OFFICE SYMBOL (If applicable)	9. PROCUREMENT INSTRUMENT IDENTIFICATION NUMBER		
8c. ADDRESS (City, State, and ZIP Code)		10. SOURCE OF FUNDING NUMBERS		
		Program Element No.	Project No.	Task No.
				Work Unit Accession Number
11. TITLE (Include Security Classification) THE ATMOSPHERIC EMISSION METHOD OF CALCULATING THE NEUTRAL ATMOSPHERE AND CHARGED PARTICLE DENSITIES IN THE UPPER ATMOSPHERE				
12. PERSONAL AUTHOR(S) Kenneth L. McElroy Jr.				
13a. TYPE OF REPORT Master's Thesis	13b. TIME COVERED From To	14. DATE OF REPORT (year, month, day) December 1992	15. PAGE COUNT 88	
16. SUPPLEMENTARY NOTATION The views expressed in this thesis are those of the author and do not reflect the official policy or position of the Department of Defense or the U.S. Government.				
17. COSATI CODES			18. SUBJECT TERMS (continue on reverse if necessary and identify by block number)	
FIELD	GROUP	SUBGROUP	Ionosphere composition modelling	
19. ABSTRACT (continue on reverse if necessary and identify by block number)				
<p>This thesis presents a method for the determination of neutral gas densities in the ionosphere from rocket-borne measurements of UV atmospheric emissions. Computer models were used to calculate an initial guess for the neutral atmosphere. Using this neutral atmosphere, intensity profiles for the N<sub>2</sub> (0,5) Vegard-Kaplan band, the N<sub>2</sub> Lyman-Birge-Hopfield band system, and the OI2972 Å line were calculated and compared with the March 1990 NPS MUSTANG data. The neutral atmospheric model was modified and the intensity profiles re-calculated until a fit with the data was obtained. The neutral atmosphere corresponding to the intensity profile that fit the data was assumed to be the atmospheric composition prevailing at the time of the observation. The ion densities were then calculated from the neutral atmosphere using a photochemical model. The electron density profile calculated by this model was compared with the electron density profile measured by the U.S. Air Force Geophysics Laboratory at a nearby site.</p>				
20. DISTRIBUTION/AVAILABILITY OF ABSTRACT			21. ABSTRACT SECURITY CLASSIFICATION	
<input checked="" type="checkbox"/> UNCLASSIFIED/UNLIMITED <input type="checkbox"/> SAME AS REPORT <input type="checkbox"/> DTIC USERS			UNCLASSIFIED	
22a. NAME OF RESPONSIBLE INDIVIDUAL Cleary, David D.			22b. TELEPHONE (Include Area code) 408-646-2828	22c. OFFICE SYMBOL PH/CL

DD FORM 1473, 84 MAR

83 APR edition may be used until exhausted  
All other editions are obsolete

SECURITY CLASSIFICATION OF THIS PAGE

UNCLASSIFIED

Approved for public release; distribution is unlimited.

The Atmospheric Emission Method of Calculating the Neutral Atmosphere  
and Charged Particle Densities in the Upper Atmosphere

by

Kenneth L. McElroy Jr.  
Lieutenant, United States Navy  
B.S., United States Naval Academy, 1985

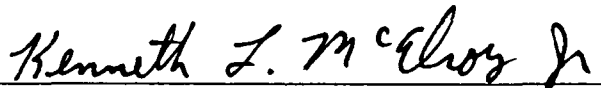
Submitted in partial fulfillment  
of the requirements for the degree of

MASTER OF SCIENCE IN PHYSICS

from the

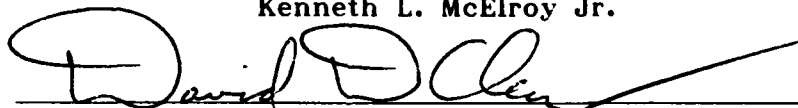
NAVAL POSTGRADUATE SCHOOL  
December 1992

Author:




Kenneth L. McElroy Jr.

Approved by:



David D. Cleary, Thesis Advisor

  
Suntharalingam Gnanalingam, Second Reader

  
Karlheinz Woehler, Chairman  
Department of Physics

## ABSTRACT

This thesis presents a method for the determination of neutral gas densities in the ionosphere from rocket-borne measurements of UV atmospheric emissions. Computer models were used to calculate an initial guess for the neutral atmosphere. Using this neutral atmosphere, intensity profiles for the  $N_2$  (0,5) Vegard-Kaplan band, the  $N_2$  Lyman-Birge-Hopfield band system, and the  $OI2972\text{\AA}$  line were calculated and compared with the March 1990 NPS MUSTANG data. The neutral atmospheric model was modified and the intensity profiles re-calculated until a fit with the data was obtained. The neutral atmosphere corresponding to the intensity profiles that fit the data was assumed to be the atmospheric composition prevailing at the time of the observation. The ion densities were then calculated from the neutral atmosphere using a photochemical model. The electron density profile calculated by this model was compared with the electron density profile measured by the U.S. Air Force Geophysics Laboratory at a nearby site.

DMC QUALITY INSPECTED 4

Accession For	
NTIS GR&I	<input checked="" type="checkbox"/>
DTIC TAB	<input type="checkbox"/>
Unannounced	<input type="checkbox"/>
Justification	
By	
Distribution/	
Availability Codes	
Dist	Avail and/or Special
A-1	

## TABLE OF CONTENTS

I.	INTRODUCTION . . . . .	1
	A. THESIS OBJECTIVES . . . . .	4
	B. THESIS OUTLINE . . . . .	4
II.	BACKGROUND . . . . .	5
	A. THE EARTH'S ATMOSPHERE . . . . .	5
	B. THE MASS CONTINUITY EQUATION . . . . .	9
	C. THE AIRGLOW . . . . .	11
	D. THE MODELS . . . . .	17
III.	THE EXPERIMENT . . . . .	24
	A. MUSTANG INSTRUMENT-CONSTRUCTION AND OPERATION .	24
	B. THE LAUNCH . . . . .	27
IV.	DATA ANALYSIS AND RESULTS . . . . .	30
	A. ANALYSIS . . . . .	30
	1. Theory . . . . .	30
	2. Procedure . . . . .	33
	B. RESULTS . . . . .	66
V.	CONCLUSIONS . . . . .	69
	A. SUMMARY . . . . .	69

B. SUGGESTIONS FOR FOLLOW-ON RESEARCH . . . . .	71
APPENDIX . . . . .	73
LIST OF REFERENCES . . . . .	79
INITIAL DISTRIBUTION LIST. . . . .	81

## I. INTRODUCTION

The earth's atmosphere has long been of interest to science. From explaining phenomenon such as the aurora borealis or northern lights to the study of weather and climate, knowledge of the atmosphere has many interesting and useful applications. In addition to the scientific community, the military considers an understanding of the atmosphere to be of extreme importance because of its profound effect on several critical systems. Specifically, the characteristics of the region of the upper atmosphere known as the ionosphere are of particular significance. Among the features of interest, the electron density is of principal concern due to its role in high frequency (HF) radio communications, satellite communications and control, and over-the-horizon radar (OTHR). Another important aspect is the naturally occurring luminescence of the atmosphere called airglow. This is significant because it offers a way to determine electron densities. Furthermore, airglow is the source of a background noise signal that affects infrared detection and tracking of ships, aircraft and ballistic missile launches by space systems. The electron density and airglow are not constant but vary due to several factors such as geographic location, time of day and solar activity.

Currently, electron densities in the ionosphere are determined by actively sounding the atmosphere with radio waves. This is accomplished in the following way. A radio wave of a certain frequency is transmitted. This signal is reflected by the ionosphere when it encounters a unique electron density which corresponds to the transmitted frequency. This frequency is called the critical frequency. The reflected signal is detected by a receiver and the time it takes to make the round trip is recorded. By multiplying half this time by the velocity of waves in free space, one can determine what is known as the "virtual" height. This is not the actual height at which the reflection occurred. The calculated virtual height is actually greater than the true height of reflection. This is because the wave group velocity in the ionosphere is less than the free-space group velocity. Techniques exist for determining the true reflection height from the virtual height. By varying the frequency, an altitude-versus-density profile can be obtained. These soundings are conducted by instruments called ionosondes and while they are accurate, they have significant disadvantages. First, these are fixed sites with limited coverage and may not be located in a particular area of interest. Second, radio sounding is only capable of providing the lower half of the electron density profile from the ground. This is because although the same electron density may occur at different altitudes, the radio wave will always reflect off the first



appropriate density it encounters i.e., the one which is at the lower altitude. Finally, ionosondes do not provide a measurement of the airglow intensity or densities of other constituents of the ionosphere.

As an alternative, one might suggest putting an ionosonde on a satellite. This might correct the coverage problem but would then only provide the upper half of the density profile and would still not give information about the airglow or the additional densities of interest. Furthermore, due to its active nature (i.e., it transmits a signal), an ionosonde would necessarily be large with a large power requirement and thus not well suited for satellite deployment.

An alternative solution is to place a spectrograph on a satellite which could record emissions from the airglow. These emissions could then be used to infer the densities of neutral and charged species from which the electron density can be determined. Because it is a passive instrument, a spectrograph is less complex, requires less power and is smaller than an active system making it ideal for satellite deployment. One such instrument is the Naval Postgraduate School's middle ultraviolet spectrograph (MUSTANG). The MUSTANG was part of a scientific payload in two successful rocket-borne experiments: one conducted in March 1990 and the other in February 1992. This thesis analyzes the data collected from the 1990 flight.

## **A. THESIS OBJECTIVES**

It is the purpose of this thesis to present a method of determining the densities of O, O<sub>2</sub> and N<sub>2</sub> by comparing data with the model calculations. Additionally, the procedure for determining the densities of the charged species and electrons will be addressed.

## **B. THESIS OUTLINE**

This thesis is divided into five chapters. Following the introduction, the second chapter gives background information necessary to understand the experiment and the analysis. Included in this chapter is a discussion of the earth's atmosphere, the airglow, and the atmospheric models. The third chapter is a brief description of the experiment including an explanation of the MUSTANG instrument's construction and how it works. Chapter IV contains the analysis of the data and the results. The final chapter discusses conclusions and suggestions for further research.

## II. BACKGROUND

Before one can understand the analysis in Chapter IV, it is important to be familiar with the concepts and models on which this analysis is based. This chapter provides the necessary background knowledge required to follow the analysis.

### A. THE EARTH'S ATMOSPHERE

The earth's atmosphere extends from the surface out to approximately 1000 km. Figure 2-1 shows a temperature versus altitude profile of the atmosphere. One can see that the atmosphere is made up of several temperature gradients. These gradients can be thought of as layers describing various temperature regions. The layer at the earth's surface is called the troposphere. Its temperature is influenced greatest by the surface temperature of the earth. This region is characterized by a negative temperature gradient. The temperature continues to decrease until an altitude of approximately 10 km. At this point, called the tropopause, the temperature starts to increase with altitude.

This next region is called the stratosphere. The rise in temperature in the stratosphere is due to heating caused by the earth's ozone layer absorbing ultraviolet light. This region has received much attention in recent years because of

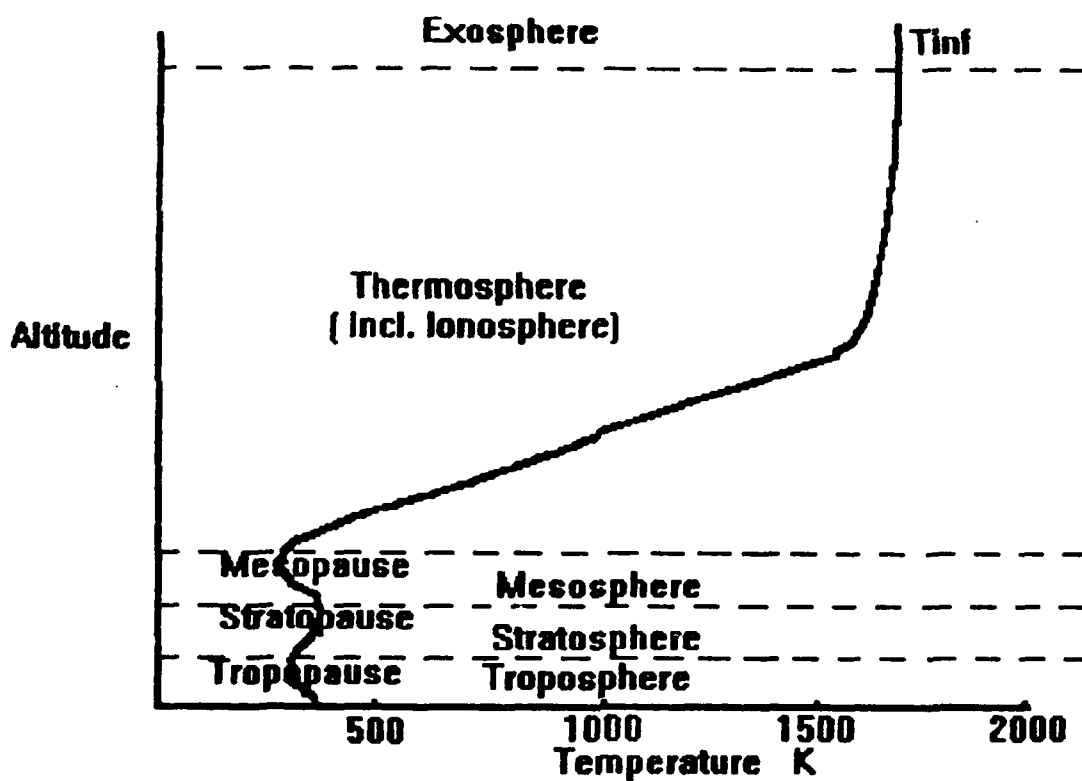


Figure 2-1 Temperature versus altitude profile of the earth's atmosphere.

the possible ozone-depleting effects of chlorofluorocarbons (CFC's) in the atmosphere. These man-made chemicals, used as solvents and refrigerants, and in many industrial processes, are known to act as a catalyst in a reaction that destroys ozone. Without ozone, the earth would not be protected from the deadly effects of ultraviolet radiation and most life forms could not survive. The ozone heating peaks at the stratopause at an altitude of around 50 km. The next region is another negative temperature gradient layer called the mesosphere. Temperature decreases until the mesopause is reached at an altitude of about 86 km. Above the mesopause is the thermosphere where temperature increases until it becomes isothermal with increasing altitude. This isothermal temperature is referred to as  $T_e$  and varies between 1000 and 1800K. This isothermal region is called the exosphere. The exosphere is characterized by extremely low densities and is the beginning of what one might call the "vacuum" of space. The region of interest for this thesis is the thermosphere.

The major constituents of the thermosphere are molecular nitrogen, molecular oxygen and atomic oxygen. Their density profiles and the temperature profile in the thermosphere make-up what is referred to as the neutral atmosphere. Radiation from the sun ionizes these species in a process called photoionization. The total ionization rate for a species at an altitude  $z$ ,  $Q(z)$ , is determined by the following equation:

$$Q^a(z) = n^a(z) \int_{\lambda_{th}}^{\infty} \sigma_i^a(\lambda) I_\lambda(\infty) e^{-\tau(\lambda, z)} CH(\theta) d\lambda \quad (2-1)$$

where:

$n^a(z)$  is the volume density of species  $a$ ,

$\sigma_i^a(\lambda)$  is the ionization cross section for species  $a$ ,

$I_\lambda(\infty)$  is the solar flux at the top of the atmosphere,

$\tau(z)$  is the optical depth at altitude  $z$ ,

$CH(\theta)$  is the Chapman function.

$\lambda_{th}$  is the threshold wavelength

The optical depth term reduces the total ionization rate at an altitude by accounting for the absorption in the atmospheric column above. The Chapman function accounts for the increasing column density as the sun moves from the zenith to the horizon.

In addition to creating ions and free electrons, photons from the sun can create excited species and energetic electrons. These energetic electrons are called photoelectrons. Photoelectrons can cause additional ionizations and excitations. Also, molecules can dissociate

as a result of photoabsorption or photoelectron impact. Chemical reactions also take place in the thermosphere which create other minor neutral and ion species. These species can also be ionized and excited. All of the above processes are called productions. Productions of one species result in the loss of others. Losses can also occur when dissociated molecules recombine or when excited particles relax back to lower energy states. The region formed by these reactions is called the ionosphere.

The ionosphere is comprised of four regions D, E, F1 and F2. These regions are based on electron density. The density of each region changes with the time of day, season and solar activity. The D-region extends from an altitude of 50 to 90 km, the E-region from 90-140 km and the F-region from 140-1000 km. The species in the ionosphere obey the one dimensional mass continuity equation (MCE) which is the subject of the following section.

## B. THE MASS CONTINUITY EQUATION

The densities of all of the constituents in the ionosphere at a given altitude obey the following mass continuity equation (MCE):

$$\frac{\partial n(Z)}{\partial t} = P - nL - \frac{\partial \phi(Z)}{\partial t}. \quad (2-2)$$

The term on the left-hand side of the equation is the change of density of a species at a given altitude with time. The first term on the right-hand side of the equation is the production processes discussed above. The second term on the right is the losses discussed above. The final term on the right is the flux term which accounts for diffusion of particles from outside the region. For most species, the entire MCE is required to calculate the density of a species at a given altitude. Some species are created and destroyed so rapidly that there is no time for them to diffuse to another altitude interval. As a result, the flux term can be ignored. In addition, for some species production and loss are in quasi-equilibrium, so the left-hand side of the equation is zero. Under these conditions, one can solve the MCE for the volume density:

$$n(Z) = \frac{P}{L}. \quad (2-3)$$

This situation is called photochemical equilibrium (PCE). In the discussion below the atmospheric emission model uses PCE in the procedure that calculates volume emission rates. It calculates the volume emission rate from the volume excitation rate. This is done in the following way. If we assume that the entire density of an excited species relaxes giving off a photon, then the volume emission rate is the density times the



Einstein coefficient, where the Einstein coefficient A is one over the lifetime of the species. The equation is:

$$VE=nA \quad (2-3a)$$

Now substituting equation (2-3) for the density and setting L equal to A (because the losses are due to relaxation) we are left with the volume emission rate equal to the production. Since each species produced is assumed to relax and give off a photon, then the volume excitation rate is equal to the volume emission rate. There are some other losses such as quenching which must also be included but they do not change the above argument because they are simply dimensionless terms that reduce the magnitude of the production. Now that the atmosphere and the MCE have been discussed, another important topic, airglow, must be addressed.

### C. THE AIRGLOW

As stated in the introduction, airglow is the naturally occurring luminescence in the atmosphere. Airglow is always present, day and night. In fact, the airglow for each of these time periods has its own name. Not surprisingly, they are the dayglow and the nightglow.

One source of the airglow is the ionosphere. When the excited atoms and molecules of the ionosphere relax to lower energy states, they give off energy in the form of a photon according to the equation:

$$E = h\nu = \frac{hc}{\lambda} . \quad (2-4)$$

The different species have several different energy levels within a state. These slightly different energy differences result in a range of wavelengths. This range of wavelengths is called an emission band. When an intensity-versus-wavelength profile is made, the result is a spectrum. In a simple case, only a single atomic or molecular emission is present for a given wavelength range. If this were the case, then the total intensity of the emission band can be determined by integrating over the wavelength range of the spectrum. Figure 2-2 shows a schematic example where one emission band produces the entire spectrum. Unfortunately, nature is much more complicated. A spectrum is the sum of the spectra of several processes. These processes produce emission bands that overlap or contaminate one another. Figure 2-3 shows the realistic case of a spectrum resulting from the sum of several contaminating emission bands. A technique called synthetic spectral fitting can be use to determine the intensity for the individual emission bands. This is described in Chapter III.

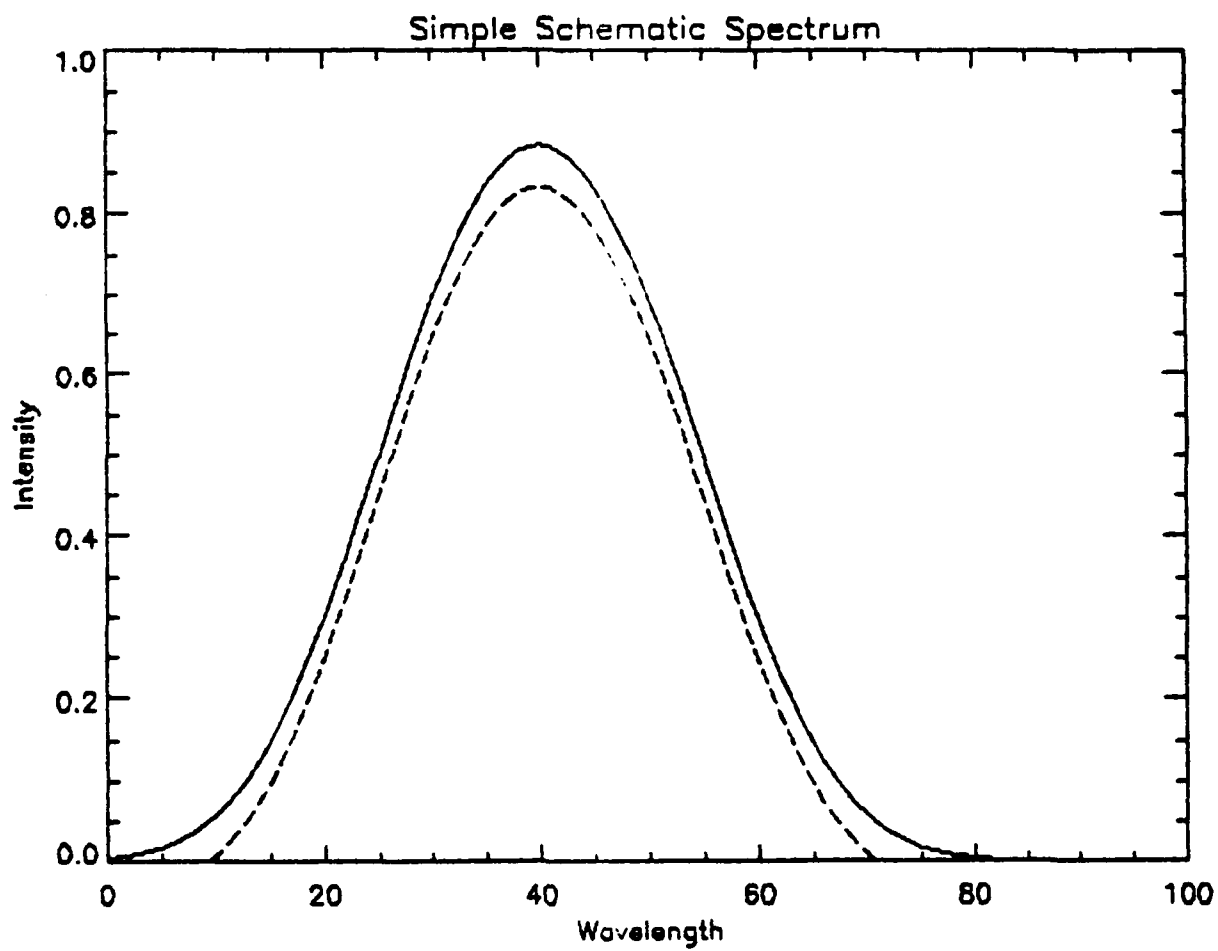


Figure 2-2 Simple schematic spectrum.

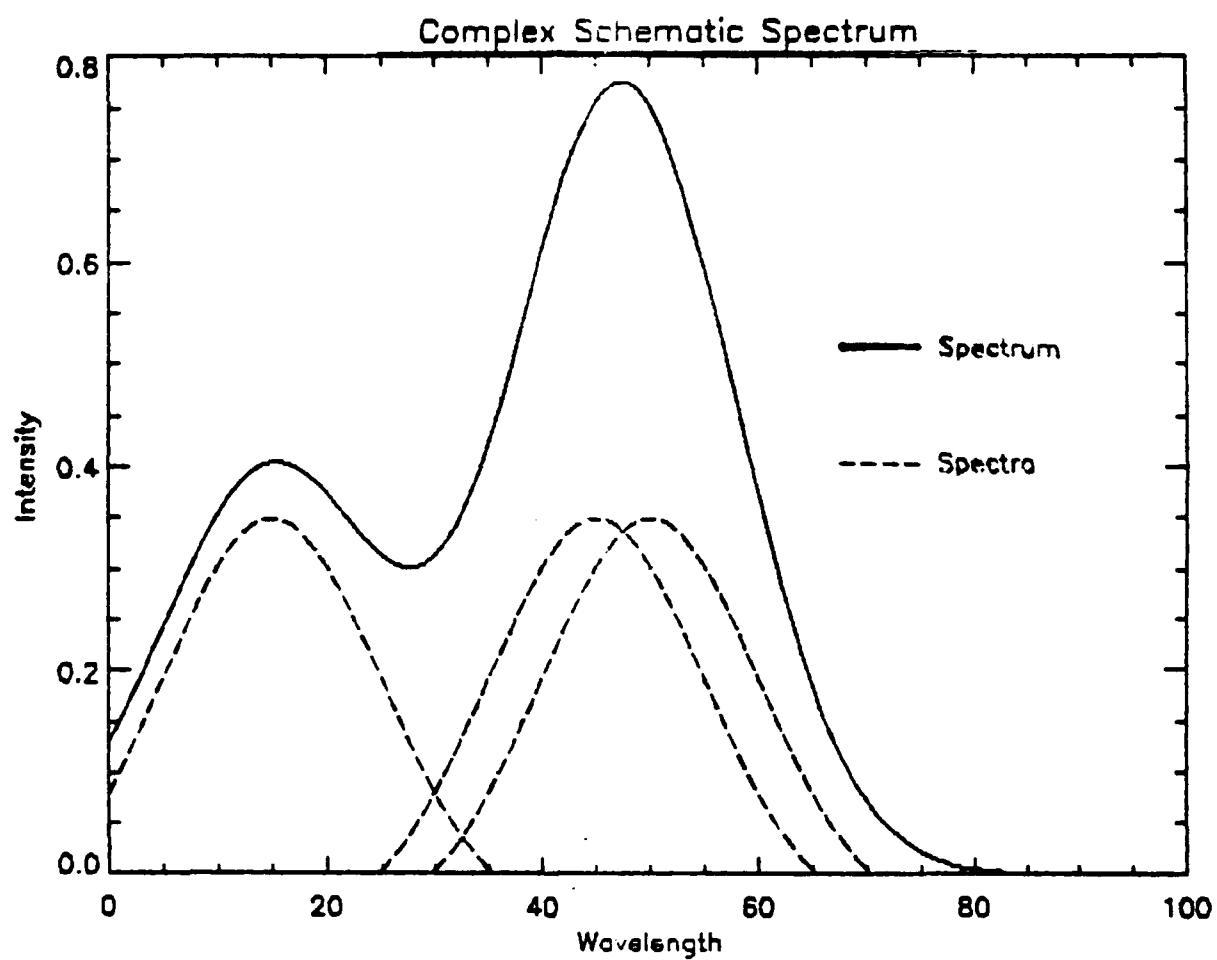
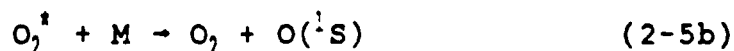


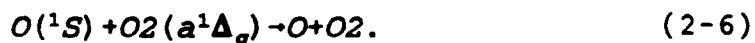
Figure 2-3 Complex schematic spectrum.

The 1990 MUSTANG data was collected during the day, therefore the emission bands used to analyze the data are dayglow emission bands. One of these emissions was the  $N_2$  (0,5) Vegard-Kaplan (VK) band. The transition for the VK band system is  $A^3\Sigma_u^+ - X^1\Sigma_g^+$ . This is a forbidden transition because excitation from the ground state, X, to the A state is forbidden by the selection rules of quantum mechanics. This does not mean that this transition cannot occur. It means that the A state cannot be populated by photoexcitation. The A state is populated in two ways: directly by photoelectron impact and indirectly by cascading from the C, B and W states (Meier, 1991). Another emission band observed in the data is  $N_2$  Lyman-Birge-Hopfield ( $a^1\Pi_g - X^1\Sigma_g^+$ ). This is another forbidden transition. The a state is populated by photoelectron impact (Meier, 1991). Unlike the VK bands, this is the only production source for LBH. The final emission observed in the data was the 2972Å line of atomic oxygen. This line is designated as OI2972Å. This is a  $^1S - ^3P$  transition and it too is forbidden.  $O(^1S)$  has different production and loss reactions for low-altitude (80-115 km) and high-altitude (above 115 km). In the low-altitude regime, the source of  $O(^1S)$  is the following reaction:



where M is taken to be either  $N_2$ ,  $O_2$ , or O so that the density [M] is equal to the sum of the densities [ $N_2$ ], [ $O_2$ ], and [O].

The sink for this altitude regime in addition to radiative relaxation is:



The source reaction has a rate coefficient of  $4.7 \times 10^{-33} (300/T)^2$   $\text{cm}^6 \text{ s}^{-1}$ . Because the proportion of  $O_2$  in the  $a$  state was unknown, the chemical loss term (Equation 2-6), is not included in the model calculations. This does not seriously affect the analysis because the low-altitude regime is below the region of interest. The source reaction also has little effect in the region of interest but was included for completeness. In the high-altitude regime the source reactions are:



Equation (2-7b) has a rate coefficient of  $2.1 \times 10^{-8} \text{ cm}^3 \text{ s}^{-1}$  for a  $O(^1S)$  yield of 10% ( $\beta=0.1$ ). Equation (2-7c) has a rate coefficient of  $5 \times 10^{-11} \text{ cm}^3 \text{ s}^{-1}$ . The sinks are the following:



The Einstein coefficients for these two sinks are  $A_{5577} = 1.06 \text{ s}^{-1}$  and  $A_{2972} = 0.045 \text{ s}^{-1}$ . The above reactions and their

corresponding rate coefficients were taken from the review by Torr and Torr (1982). The next section describes the various models used in this thesis including how to use them, what they produce, and how they use the above information.

#### D. THE MODELS

This thesis uses three main computer models in its analysis. These models are the MSIS-83 model atmosphere (Hedin, 1983), MODATM, and the atmospheric emission model which was developed for this thesis. Each will be discussed below beginning with the MSIS-83 model.

The MSIS-83 model, developed by Hedin (1983), computes a neutral atmosphere for a given set of conditions. When running this model, the user is prompted to enter several inputs. The first is IYD which is the year and date in the following format: year number and julian date i.e. YYDDD. Next is GLAT which is the latitude in degrees. Then the user is prompted to enter GLONG which is the longitude in degrees from -180 to 180. After the longitude, one enters a number for F107A. This is the three month average of the F10.7 cm flux. The F10.7 cm flux is a radio signal produced by the sun which can be detected on the ground. It gives an indication of the sun's activity. Next, the user is prompted to enter F107 which is the F10.7 flux for the day. The next input is AP which is the  $A_p$  index. This is a measure of magnetic

activity. After AP, one is prompted to enter XLT which is the local time in hours on a 24 hour clock. The last input is FRACXR which is the x-ray scaling factor and is another measure of solar activity. The values for F107, F107A, AP and FRACXR are available in NOAA publications of solar-terrestrial data. Once these parameters have been entered, MSIS-83 computes the neutral atmosphere. The neutral atmosphere is produced in 2 km increments from 86 km to 450 km. The densities of O, O<sub>2</sub>, and N<sub>2</sub> as well as the temperature profile are stored in a file named YYDDDMSIS.DAT where the YY is the year and DDD is the julian date. The .DAT extension signifies that this is a data file. For this thesis, the file created was 90089MSIS.DAT. Any further reference to this file will be made as MSIS. To avoid possible confusion, the MSIS-83 model is referred to as MSIS3. This is shortened from the IDL version of MSIS-83 which is MSIS3.PRO.

After the neutral atmosphere calculation is complete, the user is asked if he/she would like to calculate the photoelectron ionization rates for N<sub>2</sub>, O<sub>2</sub> and O, and the dissociation rate for N<sub>2</sub>. These calculations are performed by the Naval Research Laboratory (NRL) PEGFAC model (Strickland and Meier, 1982) which is called from MSIS3 but is a separate model. This creates a file 90089FLXM.PRT where the M signifies that this file corresponds to the MSIS neutral atmosphere. Further references to 90089FLXM.PRT are made as



FLXM. If one wishes to modify the neutral atmosphere, one must use the next model called MODATM.

The second model, MODATM, allows the user to modify the MSIS neutral atmosphere. The user runs MODATM after running MSIS. MODATM asks for the date in IYD format. The user is able to change the following inputs:  $T_{inf}$ ,  $T_{120}$ ,  $T_{86}$ ,  $O_{120}$ ,  $O2_{120}$ ,  $N2_{120}$  and the  $s$  parameter. The  $s$  parameter is used to calculate the temperature above 120 km. This parameter is not usually changed.  $T_{inf}$  is the isothermal temperature at the top of the temperature profile.  $T_{120}$  and  $T_{86}$  are the temperatures at an altitude of 120 km and 86 km respectively. The  $O_{120}$ ,  $O2_{120}$ , and  $N2_{120}$  inputs are the densities for these species at an altitude of 120 km. When modifying the neutral atmosphere, the MSIS values are shown as a reminder to the user. For this thesis, only the 120 km densities and  $T_{inf}$  were changed. Changing  $T_{86}$  and  $T_{120}$  has much less affect on the profile than does changing  $T_{inf}$ . MODATM uses the densities at 120 km to re-calculate the density profiles. This re-calculation is affected by both the temperature at a given altitude and  $T_{inf}$ . At lower altitudes, the effects of each are about equal. With increasing altitude,  $T_{inf}$  dominates. Therefore, only  $T_{inf}$  was adjusted for the analysis presented in this thesis. Once the changes have been made, MODATM calculates the new neutral atmosphere. It stores this information in a file called YYDDDNEU"V".DAT where the "V" is a version number to help distinguish between various runs.

For example, the first MODATM neutral atmosphere file for this thesis is 90089NEU0.DAT. These files have the same format as the MSIS file.

After the atmosphere is modified, PEGFAC is again used to calculate the photoelectron ionization rates and the  $N_2$  dissociation rate. This is done while the MODATM is being run. This information is stored in a file called YYDDDFLX"V".PRT where the "V" is the same number as the "V" in the corresponding YYDDDNEU"V".DAT file. Further references to the MODATM neutral atmosphere and flux files will be made as NEU"V" and FLX"V". Both of these files have the same format as the MSIS3 files. Now that the calculation of a neutral atmosphere has been discussed, the procedure for calculating the intensity profiles for the VK, LBH, and OI2972Å emission must be explained.

The atmospheric emission model is a collection of IDL procedures that calculates the intensity profiles for the various emissions. The IDL codes are contained in the Appendix. The procedures that actually calculate the intensity profiles are SLNTINT.PRO and OISLNT.PRO. Although the profiles have been called intensity profiles, they are actually slant intensity profiles. A slant intensity is a column intensity at a given viewing angle. Unless specified, intensity will refer to a slant intensity.

SLNTINT.PRO calculates the intensities for VK and LBH. One inputs the angle between the zenith and the instrument

viewing direction. This accounts for the difference in pathlength between the slant and vertical column intensities. For a detailed description of this see (Cleary, 1985). SLNTINT calls a procedure called GETVE.PRO. GETVE.PRO uses the following equation to calculate the volume emission rate for the (0,5) VK band:

$$VVK = \frac{((A3S+B3P+C3P/2+W3D) \times B00 \times Q05)}{1+QOx \frac{[O]}{A}} \quad (2-16)$$

In equation (2-16), A3S, B3P, C3P, and W3D are the excitation rates for the  $A^3\Sigma$ ,  $B^3\Pi$ ,  $C^3\Pi$ ,  $W^3\Delta$  states, respectively; B00 is the branching ratio for the zeroth vibrational level of the A state; and Q05 is the Frank-Condon factor for the (0,5) transition. B00 takes into account that the A state is populated by direct excitation and cascade from the B,C, and W states. The second term in the denominator accounts for losses in the A state due to quenching by atomic oxygen. QO is the oxygen quenching rate and A is the Einstein coefficient for the A state. Since the upper state for LBH is populated entirely by excitation to the a state, its volume emission rate is equal to the AlP rate. The rates are passed into GETVE from the desired FLX"V" file by the procedure GETXRATE.PRO. Densities are pass into GETVE from MSIS or the NEU"V" file by GETDENS.PRO. SLNTINT then uses a procedure called VOLSLNT.PRO to convert the volume emission rates to

slant intensities. SLNTINT passes out an altitude array and the intensity arrays for VK and LBH. By plotting the intensity arrays versus the altitude array, the intensity profiles for VK and LBH are produced. Now that the production of the VK and LBH intensity curves has been discussed, the production of the curve for OI2972Å must be addressed.

OISLNT.PRO is the model that calculates the intensity for OI2972Å. Prior to running OISLNT, one must run NOX1DIM.PRO. This is a one-dimensional photochemical model which calculates the densities for  $O_2^+$  and  $N^4S$ , and the electron density (Cleary, 1985). The  $O_2^+$  and electron densities are stored in a file called YYDDDION"V".DAT and the  $N^4S$  is stored in a file called YYDDDNNOX"V".DAT. One inputs the viewing angle and a scaling factor into OISLNT. The procedure then asks the user to specify the desired neutral atmosphere (i.e., MSIS, NEU0, NEU1, etc.). Because PCE is assumed, OISLNT calculates the volume emission rate by dividing the production terms by the loss term and multiplying this by  $A_{2972}$ . The first production term comes from the reaction given by equations (2-5a) and (2-5b). The second production term comes from equation (2-7b). The third production term comes from equation (2-7c). The loss term is the sum of the two Einstein coefficients. ( To see the actual equations for the production terms see the code for OISLNT.PRO in the Appendix ). The procedure VOLSLNT converts this volume emission rate to a slant intensity. The

resulting intensity array is plotted versus altitude giving the intensity profile for the OI2972Å emission.

Now that the background information has been covered, the experiment and analysis can be presented starting with the experiment in the next chapter.

### III. THE EXPERIMENT

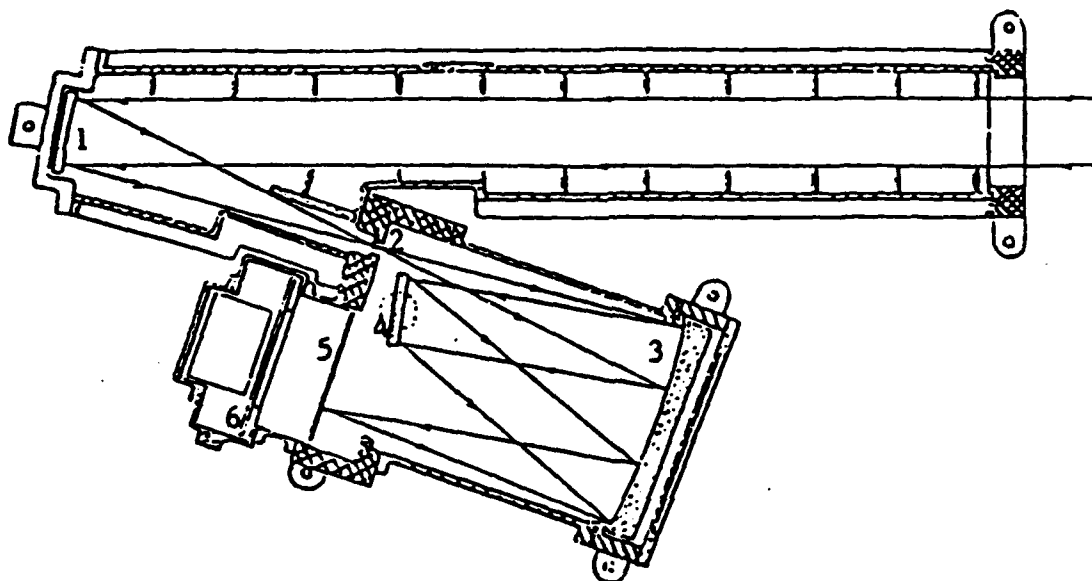
#### A. MUSTANG INSTRUMENT-CONSTRUCTION AND OPERATION

The MUSTANG instrument has three distinct parts: the telescope, the spectrograph, and the electronics interface. Figure 3-1 shows a drawing of the MUSTANG instrument. A brief description of each section and their function follows.

The first major component of the instrument is the telescope section. This is the collecting and focusing device for the instrument. The telescope is positioned off-axis from a 1/8th meter spherical mirror. Collimated light enters the telescope from the atmosphere and strikes the mirror which focuses the light at the entrance of the spectrograph. At this point, the light enters the next section.

The second section of the instrument is a modified Ebert-Fastie spectrograph. A 5mm x 140  $\mu$ m entrance slit at the focus of the telescope mirror acts as the aperture of the spectrograph. The light then diverges from this point and falls on a 1/8th meter Ebert mirror. This mirror recollimates the light onto the reflective diffraction grating. This 1200 lines/mm grating causes the light to reflect at an angle according to the following equation:

$$a \sin \theta_g = m \lambda. \quad (3-1)$$



Schematic Diagram of MUSTANG Instrument. Major components are: (1)  $1/8$ th m Telescope mirror, (2) Spectrograph entrance slit, (3)  $1/8$ th m Ebert mirror, (4) Diffraction grating, (5) ITT Image intensifier, and (6) Hamamatsu Image detector.

Figure 3-1 Schematic drawing of the MUSTANG instrument (electronic interface not shown)

The light then reflects off the Ebert mirror again and onto the ITT image intensifier in the 1800-3400Å bandwidth. Due to the diffraction grating and the mirror, light of different wavelengths falls on the image intensifier in different positions. Once calibrated, it is the position that ultimately allows an intensity/wavelength relationship to be determined. The image intensifier is comprised of a quartz input window, cesium telluride (CsTe) photocathode, two microchannel plates (MCP), a phosphor coated aluminum screen, and a fiber optic output window. The image intensifier amplifies and converts the ultra-violet light to visible light. The photocathode generates a photoelectron when it is struck by a UV photon. The electron is accelerated by an electric potential in the direction of the microchannel plates. When the electron strikes the MCP's, an electron avalanche occurs. The MCP acts as an electron multiplier producing approximately 15,000 electrons for every incoming electron. Another potential difference accelerates these electrons from the second microchannel plate to an aluminum screen. When the electrons strike the phosphor coating they cause the screen to give off visible light. The image intensifier is optically coupled to a Hamamatsu linear image sensor by its fiber optic output window and the image sensor's fiber optic input window. The image sensor uses 512 photodiodes to convert the visible light intensity to a proportional voltage.



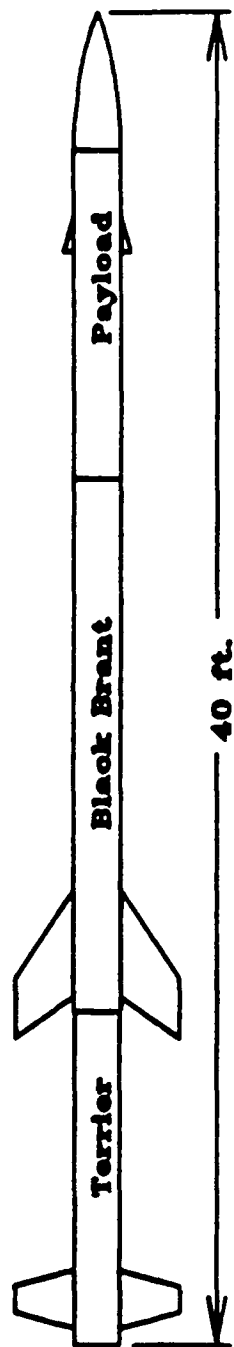
The third section of the MUSTANG is the electronic interface. This section uses an analog-to-digital converter and a first-in-first-out (FIFO) shift register to send the data to the telemetry section of the rocket. The data provided to the telemetry is sent to the ground via a RF signal. For a detailed description of the interface section see (Quint, 1991).

#### B. THE LAUNCH

The MUSTANG instrument was launched on 30 March 1990 at 1000 local time (1700 GMT) from the White Sands Missile Range, New Mexico. The launch vehicle was a NASA Terrier boosted Black Brant sounding rocket. Figure 3-2 shows a basic diagram of the sounding rocket. The MUSTANG instrument was located in the experiment section of the payload. Other sections important to the experiment were the HV section which provided the power source and the T/M section which transmitted the data back to the ground. The payload reached an apogee of approximately 320 km. Data were recorded on both the up-leg and down-leg of the flight. This experiment resulted in the collection of airglow data in the form of 8000 spectra with a wavelength range from 1800Å to 3400Å. The spectra were taken between an altitude of 100 and 320 km.

In order to determine the intensity of various emission bands, synthetic spectra of these emissions were fit to the

# **Terrier Boosted Black Brant Sounding Rocket**



## **Payload in Launch Configuration**

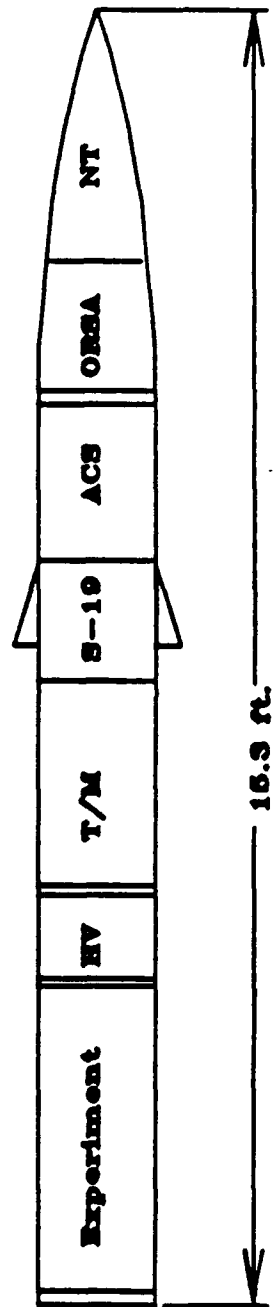


Figure 3-2 Launch vehicle block diagram.

spectra of the data. Synthetic spectra are spectra calculated for individual emission bands by models. The intensity of these spectra can be adjusted. By adding the synthetic spectra together and adjusting their intensities, fits for the data were achieved. Once these fits were obtained, the intensities for the various emissions were assumed to be the intensities of their corresponding synthetic spectra.

The above process was performed by Walden (1991) using the  $N_2$  (0,5) Vegard-Kaplan,  $N_2$  Lyman-Birge-Hopfield, 2972Å atomic oxygen and several other emissions. The 8000 spectra were averaged into 25 altitude bins. Each bin covered a 10 km altitude range. As a result, the intensity versus altitude profiles were determined for these emissions for the 1990 flight. The profiles for the VK, LBH, and OI2972Å emissions were used in the atmospheric emission model to determine the neutral atmosphere.

Now that the background information and the experiment have been discussed the data analysis and results can be addressed.

#### IV. DATA ANALYSIS AND RESULTS

##### A. ANALYSIS

###### 1. Theory

The technique used to analyze the data is simple. One adjusts the inputs to the model until a satisfactory fit is obtained. The neutral atmosphere that produces this fit is assumed to represent the conditions at the time of the observations. In this thesis, unless otherwise stated, the data refers to the intensity profiles from the analysis performed by Walden (1991).

As a starting point, one uses the MSIS3 model to generate a neutral atmosphere and the atmospheric emission model to calculate an intensity profile for a specific emission. The photoelectron excitation rates required by the model to produce intensity profiles for emission bands such as the Lyman-Birge-Hopfield, Vegard-Kaplan, and atomic oxygen 2972Å are created by the PEGFAC and stored in the FLXM data file. One then compares the intensity profile of the data with that of the model. If the two curves fit, then the atmospheric densities of O, O<sub>2</sub>, and N<sub>2</sub> (also written as [O], [O<sub>2</sub>], and [N<sub>2</sub>]) are the same as those calculated by MSIS3 and stored in the MSIS data file.

If the model calculation does not agree with the data, then one must modify the neutral atmosphere by adjusting  $T_{inf}$  and/or  $[O]$ ,  $[O_2]$ , and  $[N_2]$  at 120 km using MODATM. The model is again used to generate an intensity profile and the effect that these changes have on the calculated profile is noted. It was found that an increase(decrease) in  $T_{inf}$  increases(decreases) the scale height of the calculated emission while increasing(decreasing)  $[N_2]$  shifts the curve up(down) in altitude and increasing(decreasing)  $[O]$  shifts the profile right(left). It was also found that changing  $[O_2]$  has little effect in the region of interest. These effects are consistent with the findings of Mack (1991). This process of adjusting the neutral atmosphere and comparing it with the data could lead to several sets of inputs which fit the data reasonably well in shape but not necessarily magnitude.

Although the general shape of the profiles may agree, it may be necessary to multiply the curve by some constant to fine tune the fit. This is called a scaling factor. Scaling factors are generally small--usually less than ten. They are significant because they have the effect of increasing the solar EUV flux used by MSIS3 and MODATM to predict the neutral atmosphere. For example, a scaling factor of 1.5 would increase the solar EUV flux by 50% which would have the end result of increasing the intensity by 50%. In addition, the same scaling factor should be required to fit all other emission bands since the solar flux is the same for each. An

inconsistency in the scaling factor indicates that the set of inputs used to produce the neutral atmosphere is suspect. The connection between intensity and the solar flux was described in Chapter II.

Once a set of likely neutral atmospheres has been determined, then another emission is selected for examination. Intensity profiles for this emission are calculated using the atmospheric emission model and each of the different sets of inputs. The profiles for this second emission are compared with the data as before. Some of these calculated profiles will fit the data reasonably well while others will have the wrong shape, scale height, etc. and can be eliminated. One continues this process of selecting an emission, calculating the intensity curves using the remaining input sets and eliminating ones that produce curves that do not fit the data until only one combination remains. The density profiles stored in the NEU"V" file which corresponds to these initial conditions are those of the neutral species for that day and time. The density profiles of the various species of ions, excited species, and the electrons can then be calculated using NOX1DIM.PRO and the corresponding MSIS or NEU"V" file. These profiles are stored in 90089ION"V".DAT (90089NOX"V".DAT for the excited species) where again the "V" is either M for MSIS or the version number from MODATM.

Now that a general description of the theory has been discussed, the step-by-step procedure used to analyze the data can be presented.

## 2. Procedure

To begin the analysis, the MSIS3 program was run using the following values:  $AP=69$ ,  $F10.7=186.5$ ,  $\text{ave } F10.7=189.9$  and  $x\text{-ray scaling} = 5$  (Cleary, private communication, 1992). This produced a  $T_{\text{inf}}=1255\text{K}$  and the following densities at 120 km:  $[O]=8.8E10 \text{ cm}^{-3}$ ,  $[O_2]=4.4E10 \text{ cm}^{-3}$ , and  $[N_2]=3.2E11 \text{ cm}^{-3}$ . It also created the data files MSIS and FLXM. Figure 4-1 is a comparison of the LBH curve generated by the atmospheric emission model using the above inputs with the data. As one can see, the calculated intensity profile for LBH shows a reasonable fit with the data both in scale height and in shape above approximately 120 km when scaled. The scaling factor necessary to get a good fit is 1.8. Although the model gives profile information below 120 km, no attempt to fit the prediction to the data was made at lower altitudes for the following reason. Below 120 km, it is difficult to distinguish between the LBH bands and the brighter NO emissions. This caused the fit between the spectra and the data to be less certain. The intensity profile for the data obtained from the fit in the region below 120 km is therefore less reliable.

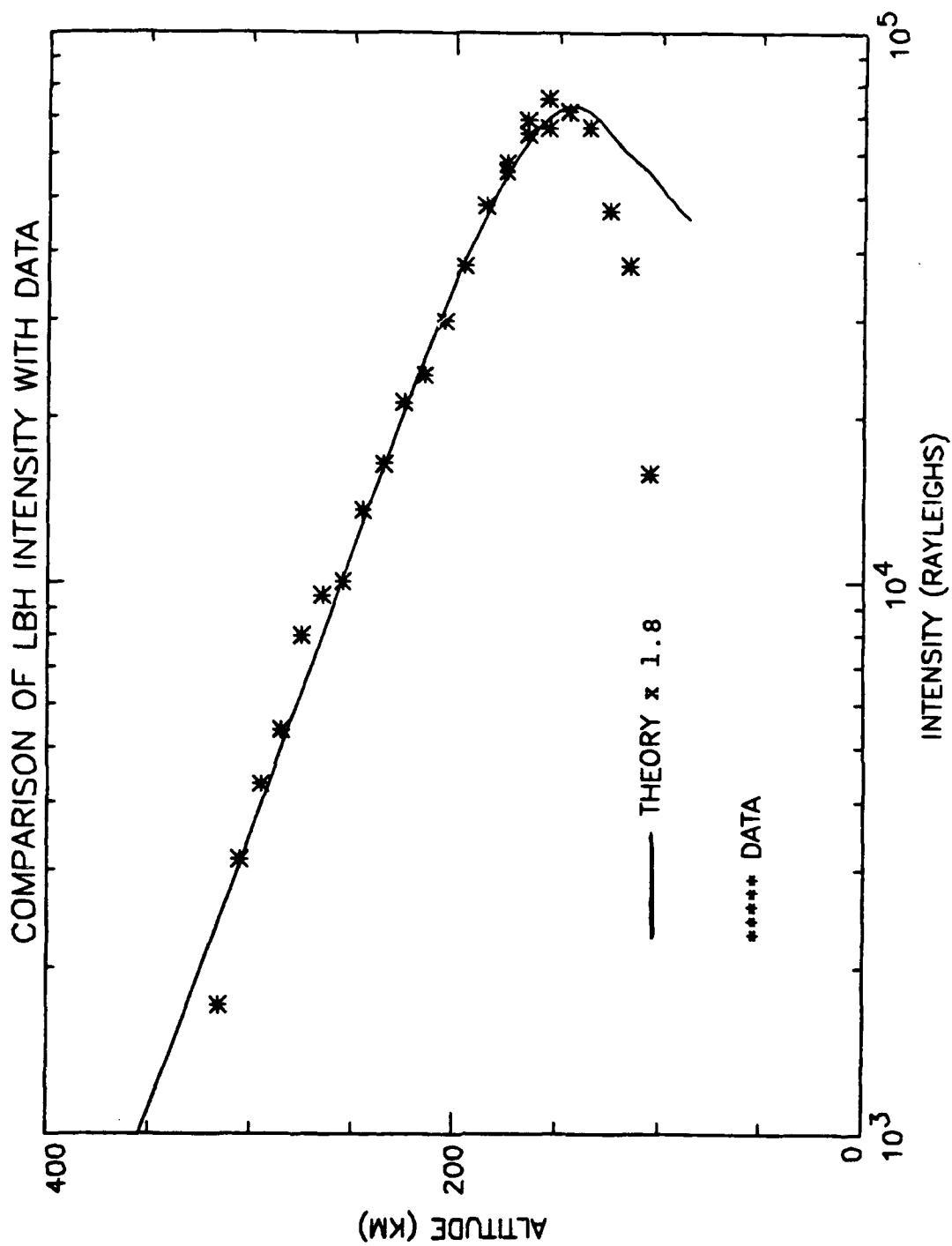


Figure 4-1 Comparison of the data with the model intensity profile for LBH using MSIS values:  $[O]_{120}=8.8E10 \text{ cm}^{-3}$ ,  $[O_2]_{120}=4.4E10 \text{ cm}^{-3}$ ,  $[N_2]_{120}=3.2E11 \text{ cm}^{-3}$  and  $T_{inf}=1255K$ .



Even though the above trial produced a good fit, two other combinations of inputs were tried. These sets were suggested by Mack (1991). The purpose of this was to test whether either of these two neutral atmospheres would lead to a fit when compared with the data from Walden's analysis. To do this, MODATM was used to change the value of  $T_{inf}$  to 1500K and to reduce the MSIS3 [O] at 120 km by 27% and increase the MSIS3 [O<sub>2</sub>] and [N<sub>2</sub>] at 120 km by 5% and 30% respectively. This trial produced NEU0 and FLX0. These changes were made based on values suggested on page 82 of the report by Mack (1991). The effects of these modifications can be seen by the comparison of the LBH intensity curves of the atmospheric emission model with the data shown in Figure 4-2. The curve produced from these values has the wrong scale height and it also required scaling which was not needed by Mack.

The other possible combination used  $T_{inf}=1700K$  and the input values for the neutral species densities at 120 km as suggested on page 83 of Mack (1991). These values represent a 48% reduction in [O], a 6% increase in [O<sub>2</sub>] and the MSIS3 value for [N<sub>2</sub>] at 120 km. A run using these values was performed and the calculations were stored in NEU1 and FLX1. Figure 4-3 shows the intensity profile generated by the atmospheric emission model for LBH produced by this modification and the data profile. One can see that the curve produced using these inputs also does not agree with the data.

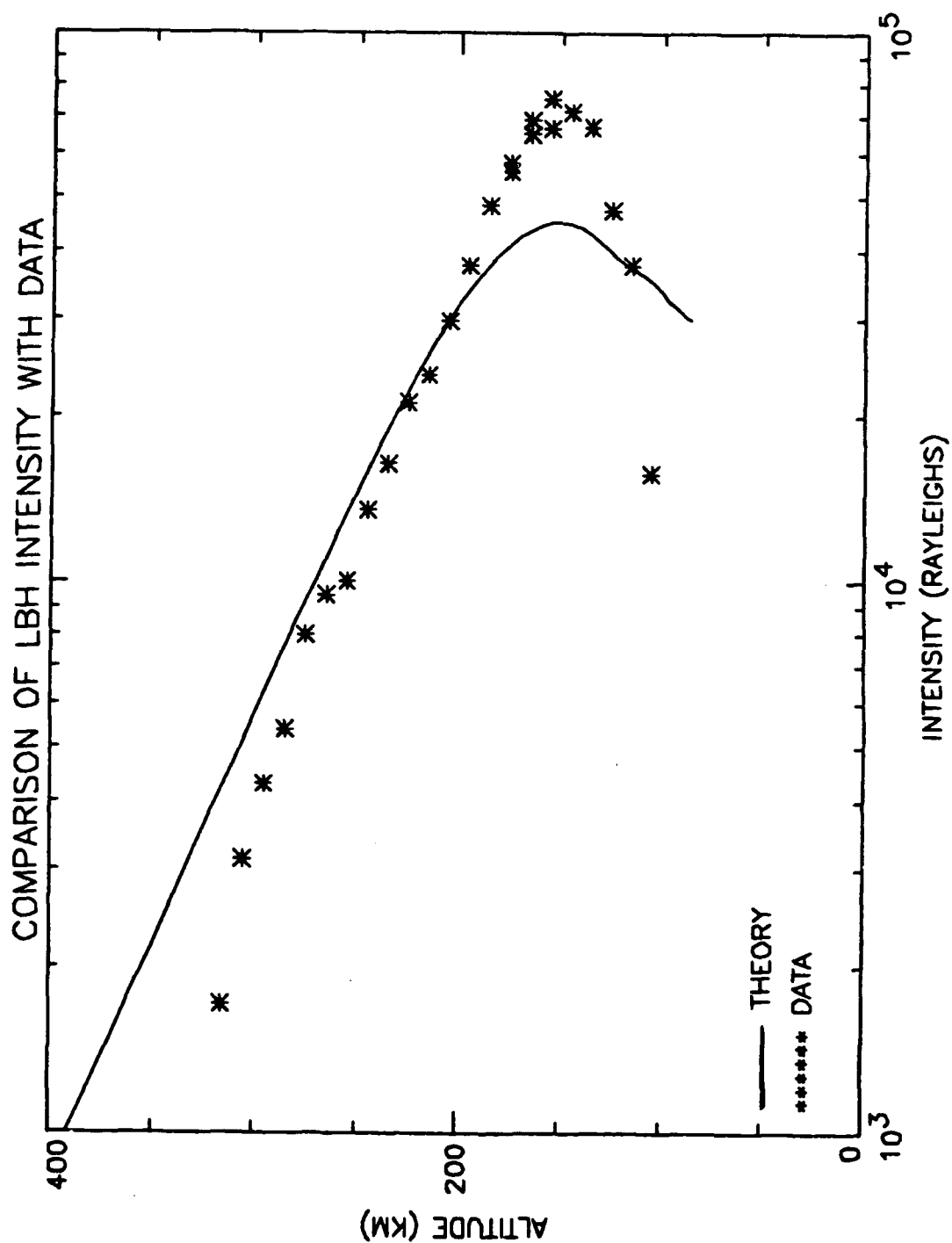


Figure 4-2 Comparison of the data with the model intensity profile for LBH using MODATM values:  $T_{inf}=1500K$ ,  $-27\%$   $[O]_{120}$ ,  $+5\%$   $[O_2]_{120}$  and  $+30\%$   $[N_2]_{120}$ .

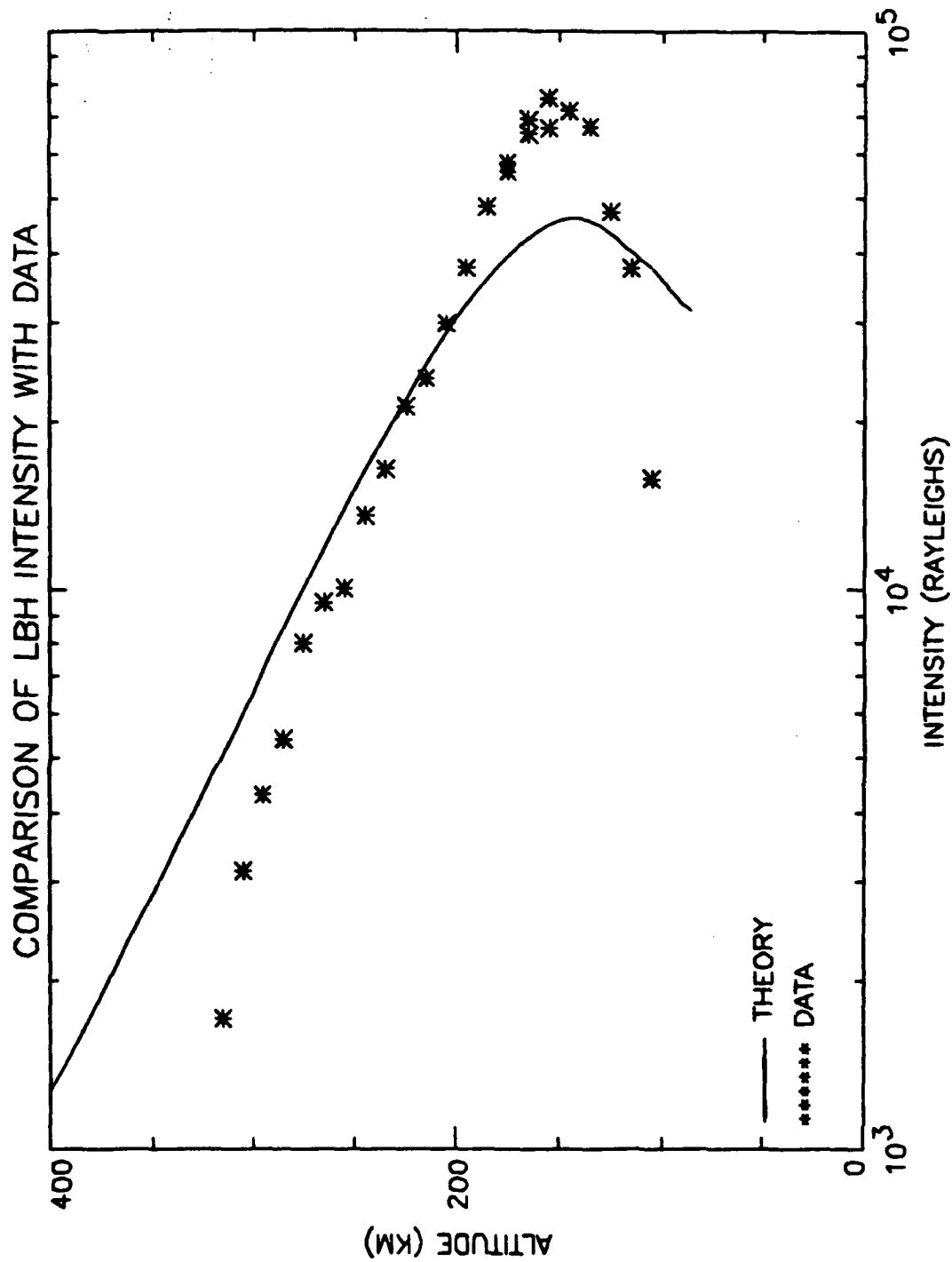


Figure 4-3 Comparison of the data with the model intensity profile for LBH using MODATM values:  $T_{inf}=1700K$ ,  $-48\%$   $[O]_{120}$  and  $+6\%$   $[O_2]_{120}$ .

When compared with the intensity profiles for the data from (Walden, 1991), neither set of inputs fit the data. The fact that this analysis rejected the sets of possible inputs suggested by Mack (1991) can be explained in the following way. The intensity profiles for the data were determined by fitting synthetic spectra to the data spectra. Mack (1991) used only part of the MUSTANG wavelength range while the later analysis by Walden (1991) used the full wavelength range of the instrument. Analysis over a smaller wavelength range, which includes fewer emission features, is much more sensitive to large fluctuations in the intensity than analysis over a larger range. One can imagine that if a fit was performed at the only large data spike in an otherwise even spectra, the fit would be poor for the whole spectral range. Because of this, the data profiles produced by Walden (1991) are considered more accurate. The input sets suggested by Mack (1991) do not fit the improved data curves. Therefore they were rejected.

Since the original curve from MSIS/FLXM showed better agreement than either of the profiles from NEU0/FLX0 and NEU1/FLX1, an attempt was made to fit the data using the original  $T_{inf}=1255K$  while varying the neutral densities. Pursuit of a fit using NEU0/FLX0 or NEU1/FLX1 was not continued because the scale heights of these curves did not match the data. It was apparent that their  $T_{inf}$  values were

not correct and that the modification of the densities would not result in a fit.

Continuing the analysis, MODATM and the original MSIS3 values for  $T_{inf}$ ,  $[O_2]_{120}$ , and  $[N_2]_{120}$  were used. Only half of the  $[O]_{120}$  was used and NEU2/FLX2 was created. From Figure 4-4 which shows this LBH intensity profile and the data, one can see that this modification produced a curve with a peak intensity which was a little too low. As stated earlier, increasing  $[N_2]_{120}$  causes the peak intensity of the model calculation to occur at a higher altitude. The next trial makes use of this effect. To create the files NEU3 and FLX3, MODATM was run with all NEU2/FLX2 values except  $[N_2]_{120}$  was increased by 30%. The intensity profile produced with these values is shown in Figure 4-5. The effects of this change can be seen by comparing Figures 4-4 and 4-5. This last run, when scaled by 1.3, showed excellent agreement between the model and the data. At this point, two input sets, MSIS and NEU3, still look capable of producing the correct neutral atmosphere so it was necessary to choose another emission and to continue the analysis.

The next emission profile examined was the (0,5) Vegard-Kaplan band. When the model intensity profiles using MSIS and NEU3 were compared with the data, neither of the profiles for VK agreed well with the data as seen in Figures 4-6 and 4-7. Both curves fit the peak intensity of the data well. However, moving above the peak, the agreement for both

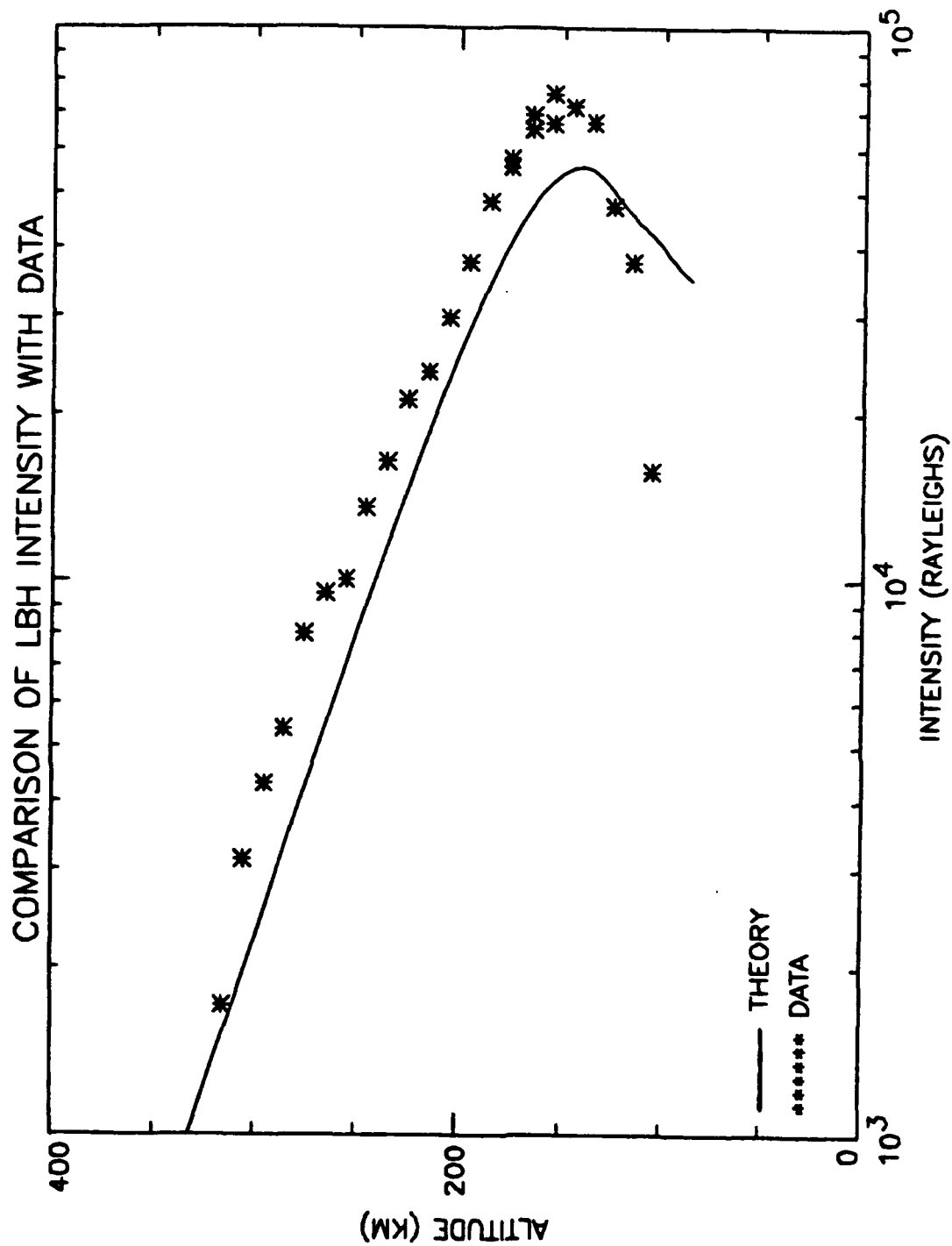


Figure 4-4 Comparison of the data with the model intensity profile for LBH using MODATM values:  $T_{inf}=1255K$  and  $-50\%$  [0].

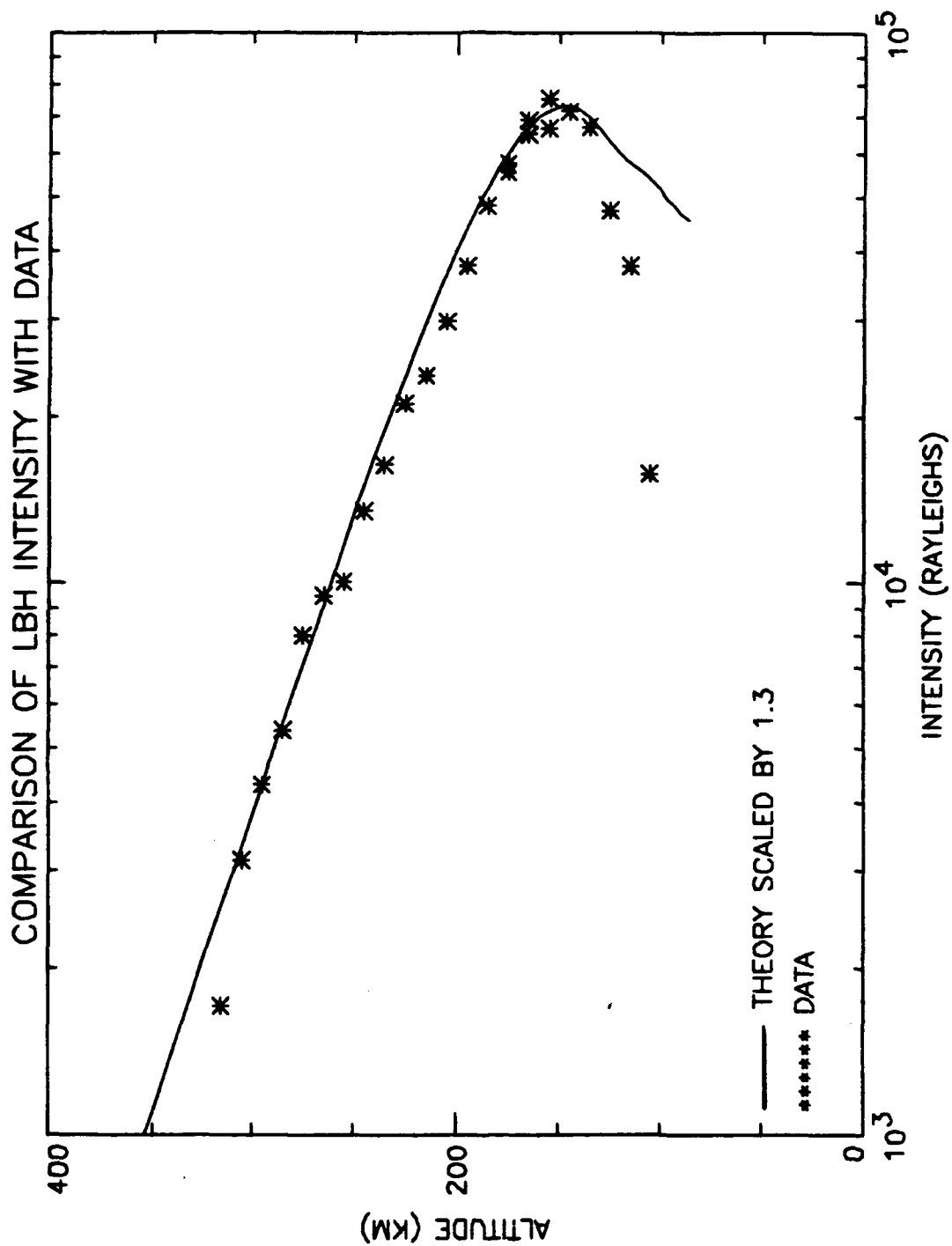


Figure 4-5 Comparison of the data with the model intensity profile for LBH using MODATM values:  $T_{inf}=1255K$ ,  $-50\% [O]_{120}$ , and  $+30\% [N_2]_{120}$ .

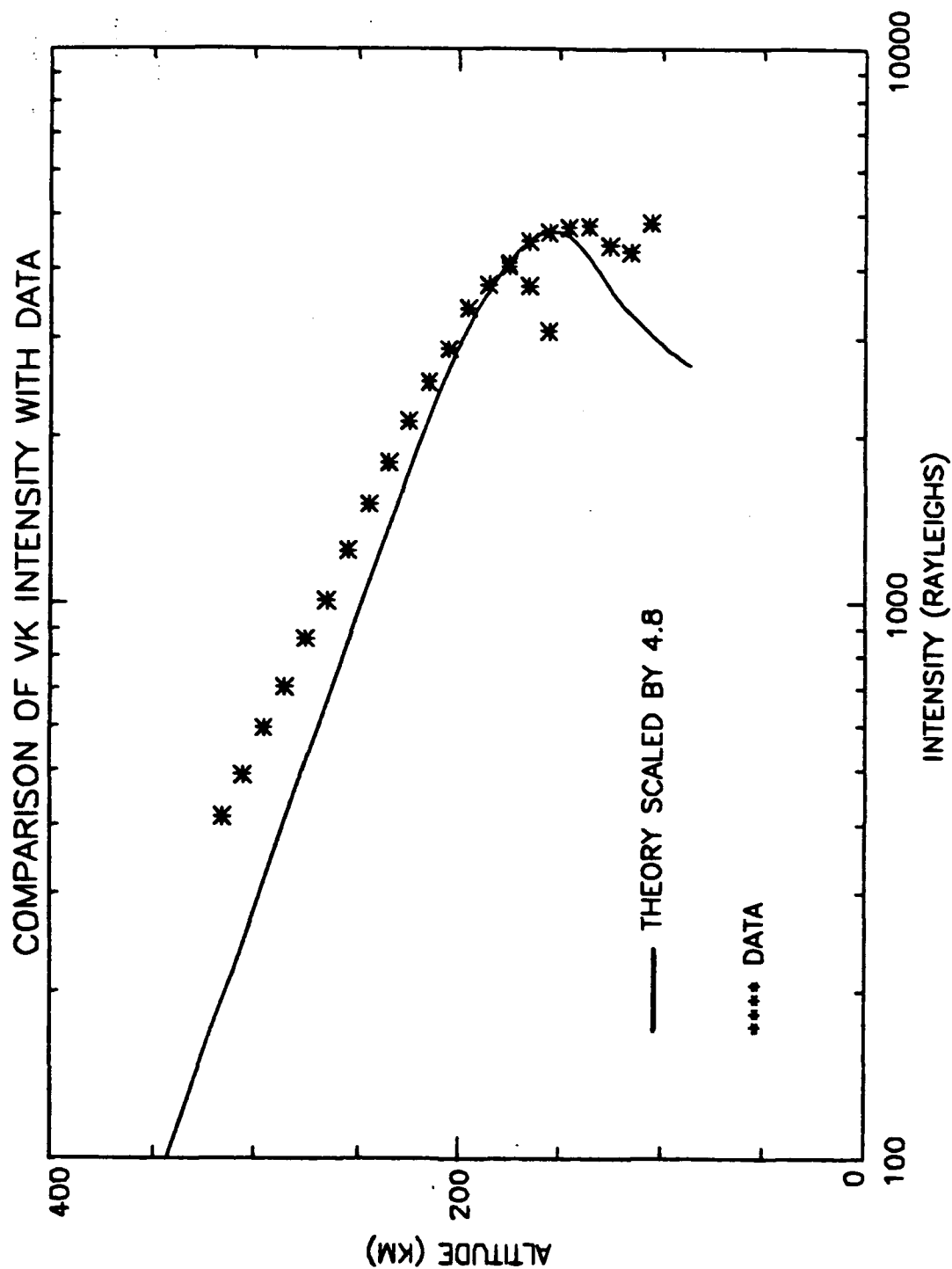


Figure 4-6 Comparison of the data with the model intensity profile for VK using MSIS values:  $T_{inf}=1255K$ ,  $[O]_{120}=8.8E10 \text{ cm}^{-3}$ ,  $[O_2]_{120}=4.4E10 \text{ cm}^{-3}$ , and  $[N_2]_{120}=3.2E11 \text{ cm}^{-3}$ .



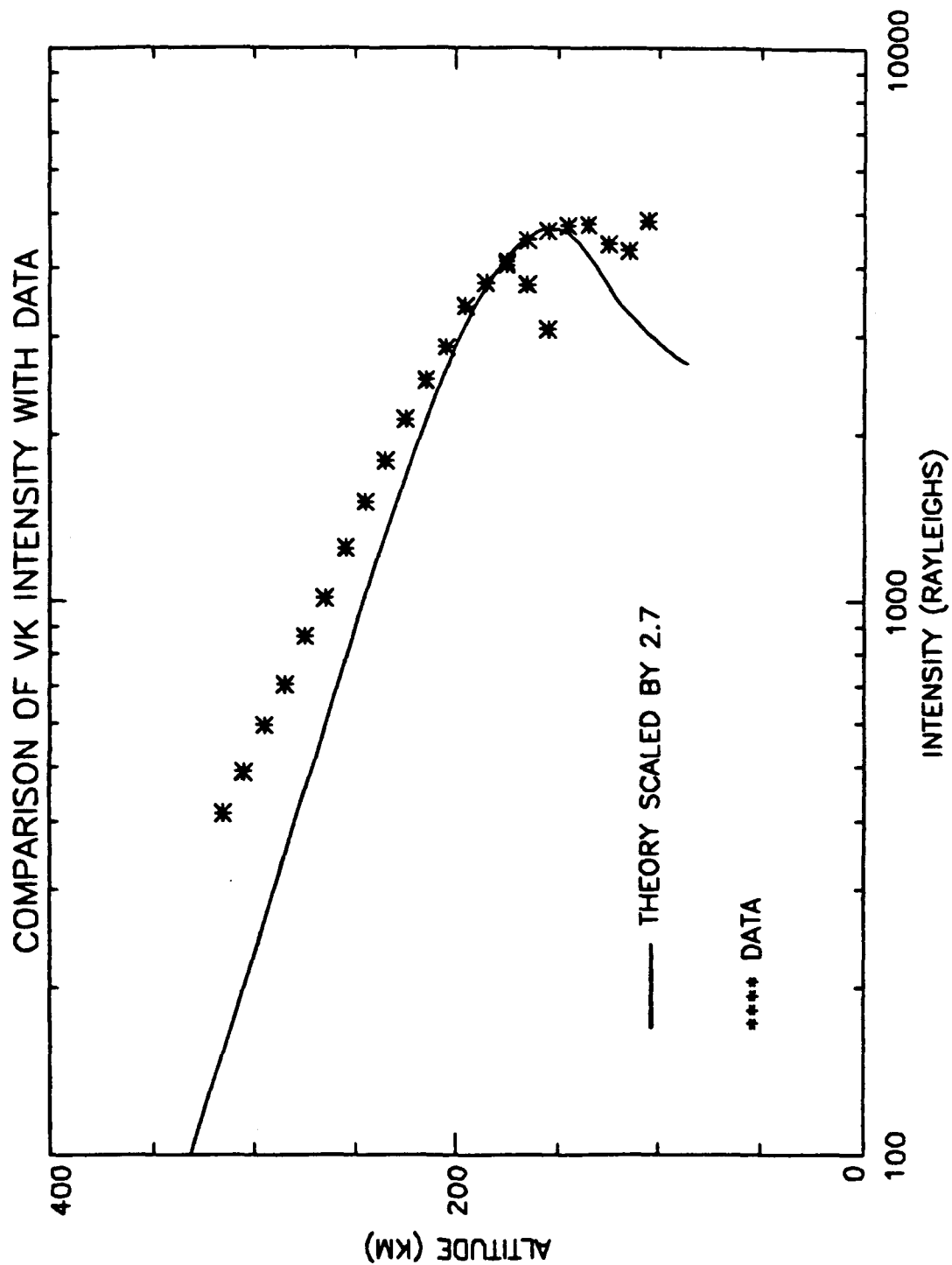


Figure 4-7 Comparison of the data with the model intensity profile for VK using MODATM values: -50% [O]<sub>120</sub>, +30% [N<sub>2</sub>]<sub>120</sub> and T<sub>inf</sub>=1255K.

worsened due to a difference in the scale heights. Furthermore, in order to get the fit at the peak, it was necessary to scale the curve for MSIS by 4.8 and 2.7 for NEU3. Because the solar flux is the same for all emissions, the scaling factor should be the same regardless of the emission being examined. Therefore, any large variation in the scaling factor is an indicator that that set of inputs should be considered suspect.

Because neither MSIS nor NEU3 lead to a good fit, the order in which the emission features were fitted was changed. The intensity profile of the VK band is more reliable data than the profile for the LBH because the signal-to-noise ratio of the VK data was greater. As a result, reversing the order of the analysis to VK and then LBH is a better approach. Furthermore, this ordering is superior because the model for VK is more complicated due to a greater number of production terms. This causes more variables to be constrained by analyzing the VK bands first.

To begin the analysis using VK, a value of  $3\text{E-}11$  for the atomic oxygen quenching rate coefficient was determined by taking the average of the values reported by Piper et al. (1981), Thomas and Kaufman (1985) and De Souza et al. (1985). Also, an estimate of 0.125 for the zero vibrational level branching ratio was used. This was determined in the following manner. The first 8 vibrational levels (0 through 7) for  $\text{A}^3\Sigma$  (no quench) from Figure 22 of (Cartwright, 1978)

appear to be of the same order of magnitude. Therefore, the branching ratio for the zeroth vibrational level was estimated to be  $1/8$  of the total relative number density of these states or 0.125. Using these values in the atmospheric emission model, previously rejected runs were re-evaluated. NEU0/FLX0 and NEU2/FLX2 were again rejected because the curves showed poor agreement with the data (see Figures 4-8 and 4-9). On the other hand, the run using NEU1/FLX1 fit the data well except for a slight difference in the scale height which was only a little too high as seen in Figure 4-10. Although the calculations using MSIS/FLXM and NEU3/FLX3 were found to be poor as stated above, they were the best two fits from the original analysis attempt. Therefore, they were not immediately rejected. In addition, these runs, like the NEU1/FLX1 trials, fit pretty well at the peak intensity but differed from the data elsewhere due to the scale height difference.

One way in which the scale height can be increased is to increase the atomic oxygen quenching rate coefficient. Figure 4-11 shows a VK intensity curve using  $3E-11$  and one using  $9E-11$ . This illustrates the effect that this change has on the VK intensity profile. This higher coefficient was suggested by Sharp (1971). Unfortunately, a change in the scale height is not the only effect that increasing the atomic oxygen quenching rate has on the VK profile. Figure 4-11 also shows that by increasing the rate, the peak intensity occurs

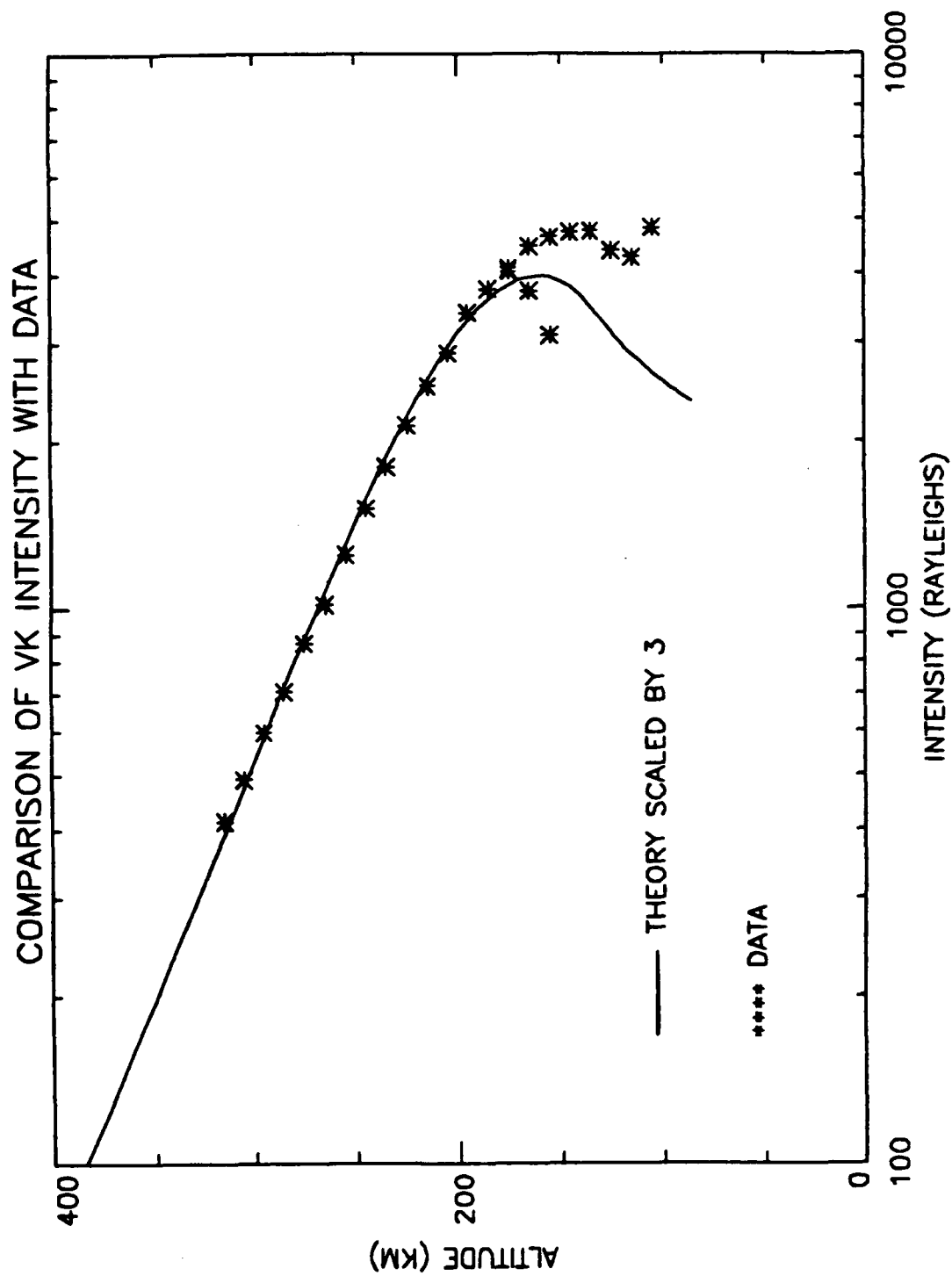


Figure 4-8 Comparison of the data with the model intensity profile for VK using MODATM values:  $T_{inf}=1500K$ ,  $-27\%$   $[O]_{120}$ ,  $+5\%$   $[O_2]_{120}$  and  $+30\%$   $[N_2]_{120}$ .

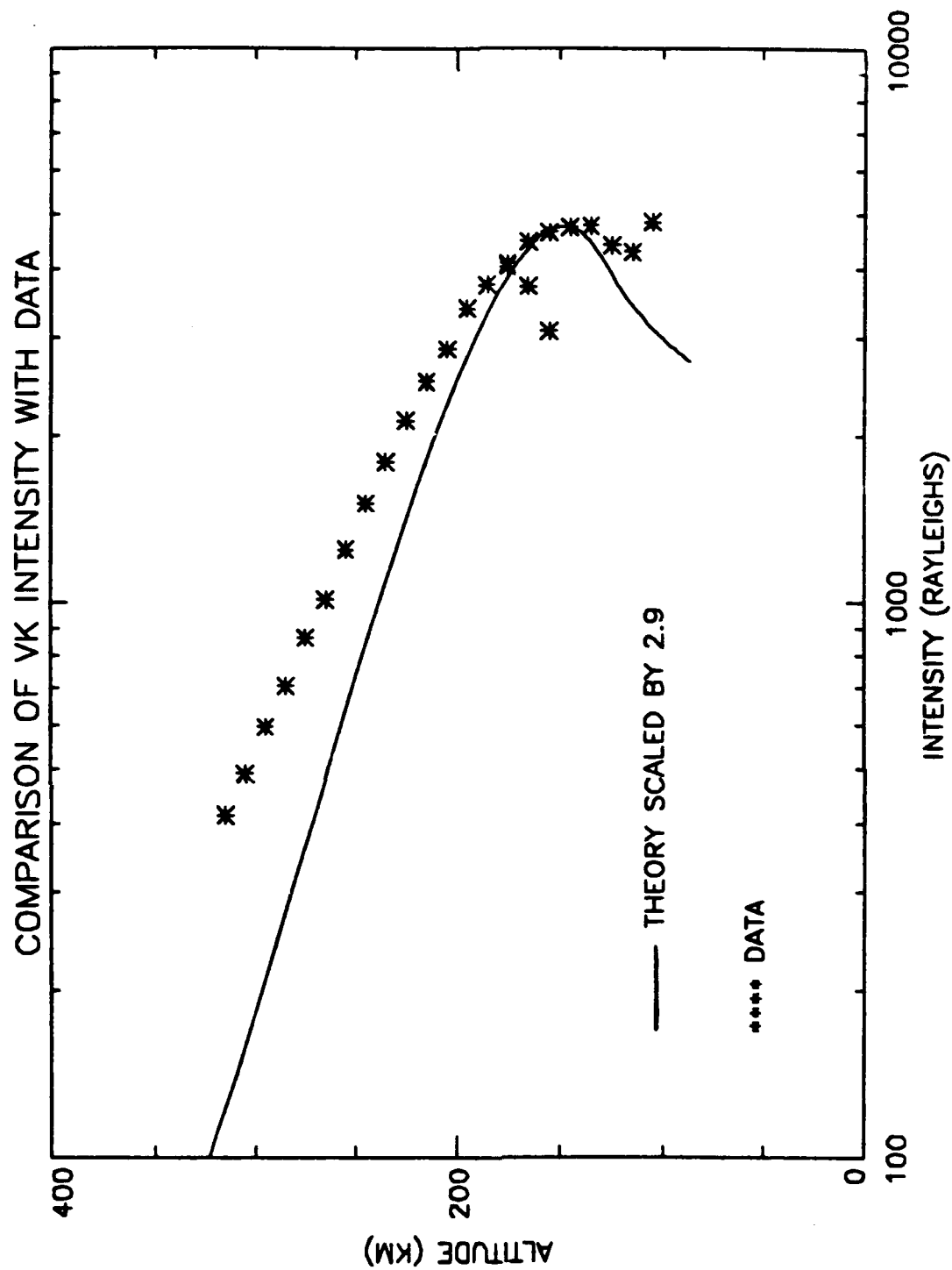


Figure 4-9 Comparison of the data with the model intensity profile for VK using MODATM values:  $T_{inf}=1255K$  and  $-50\% [O]_{120}$ .

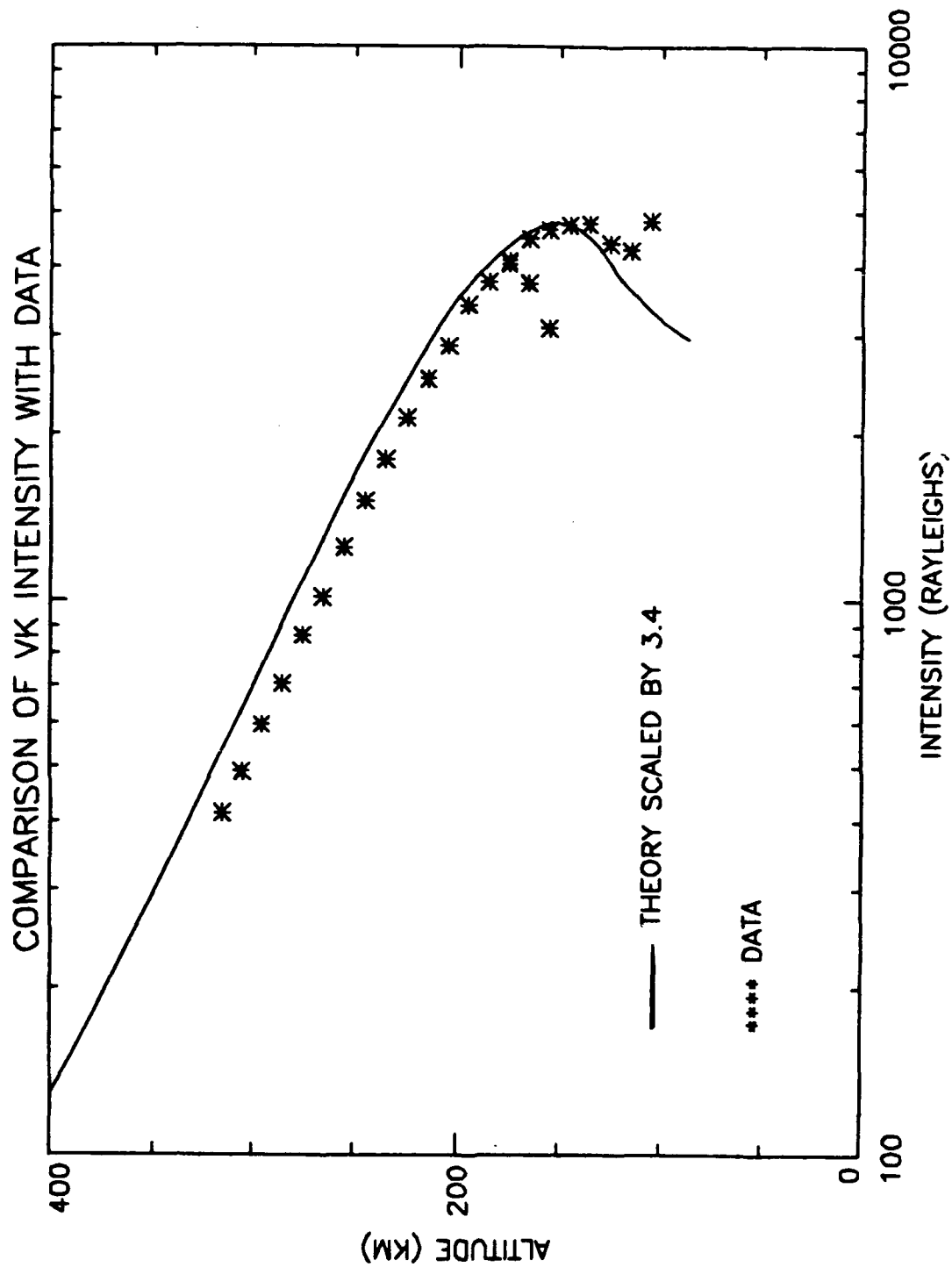


Figure 4-10 Comparison of the data with the model intensity profile for VK using MODATM values:  $T_{inf}=1700K$ ,  $-48\%$   $[O]_{120}$  and  $+6\%$   $[N_2]_{120}$ .

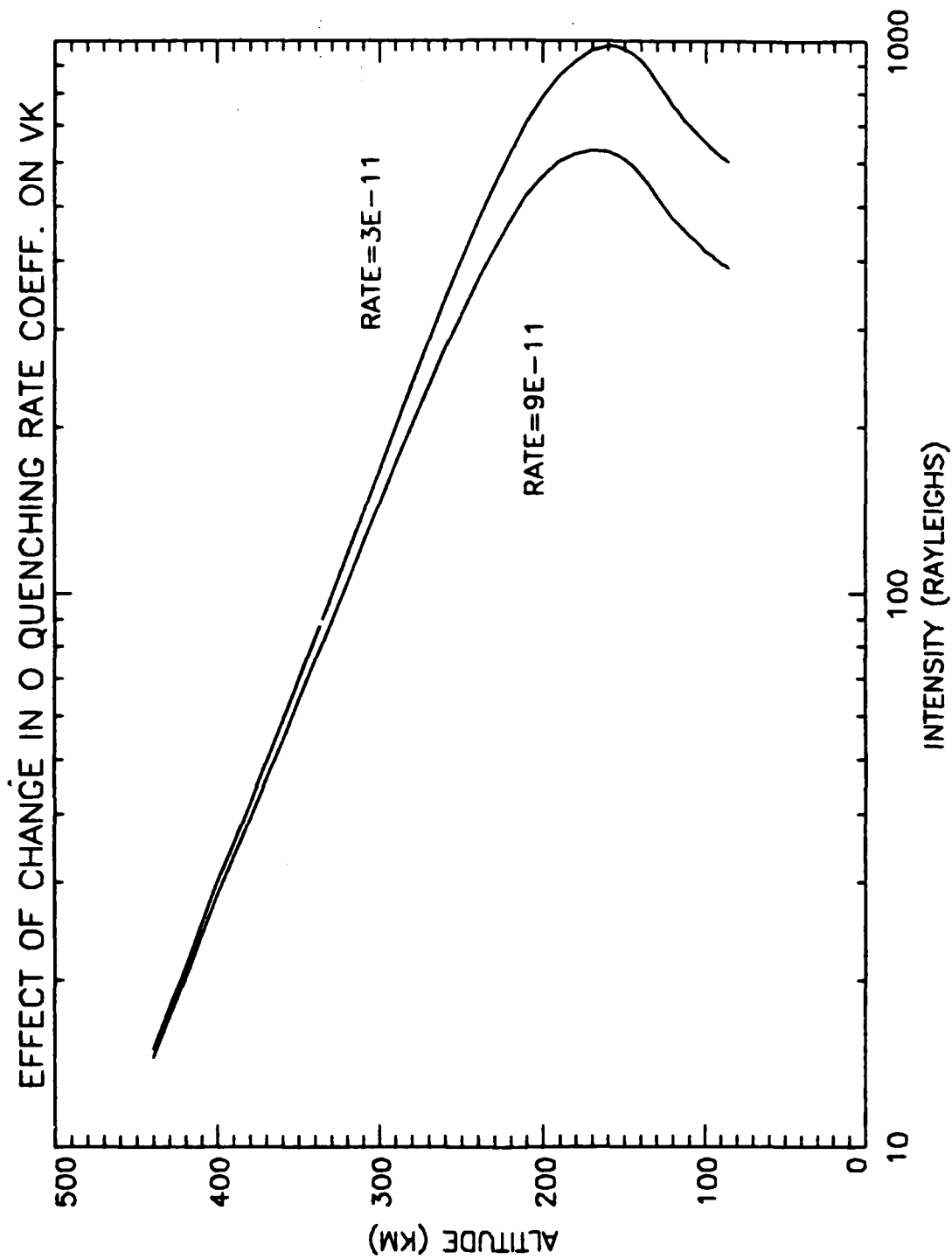


Figure 4-11 Effect of changing the atomic oxygen quenching rate coefficient on VK intensity profile.

at a higher altitude and the overall intensity drops. This drop in intensity is most pronounced at the peak. The MSIS/FLXM, NEU1/FLX1, and NEU3/FLX3 runs were repeated using the higher quenching rate coefficient but the fits were again poor and they required an even larger scaling factor.

Another way to increase the scale height of the VK emission profile is to increase  $T_{inf}$  as was discussed earlier. Taking this into consideration, one might guess that a slightly lower  $T_{inf}$  might improve the fit using NEU1/FLX1. Several attempts were made using  $T_{inf}=1600K$ , a quenching rate coefficient of  $9E-11$  and various combinations of neutral densities at 120 km. These trials were all variations of NEU4/FLX4 and none produced the desired effects (see Figures 4-12 through 4-14). Scaling was attempted to fit the peak. Next, the quenching rate coefficient was changed back to  $3E-11$  and better results were achieved as one can see from Figure 4-15. In this run, the peak intensity was too high so NEU5/FLX5 was created using  $T_{inf}=1600k$ , half the MSIS3  $[O]_{120}$  value and increasing the MSIS3  $[N_2]_{120}$  by 30%. This produced better scale height agreement but the altitude for the peak intensity was still a little too high as one can see from the intensity profile in Figure 4-16. The final run for VK used the NEU5/FLX5 values except the peak was lowered by lowering the  $[N_2]_{120}$  back to the original MSIS3  $[N_2]_{120}$ . This run was called NEU6/FLX6 and gave an excellent fit when scaled by 3.25



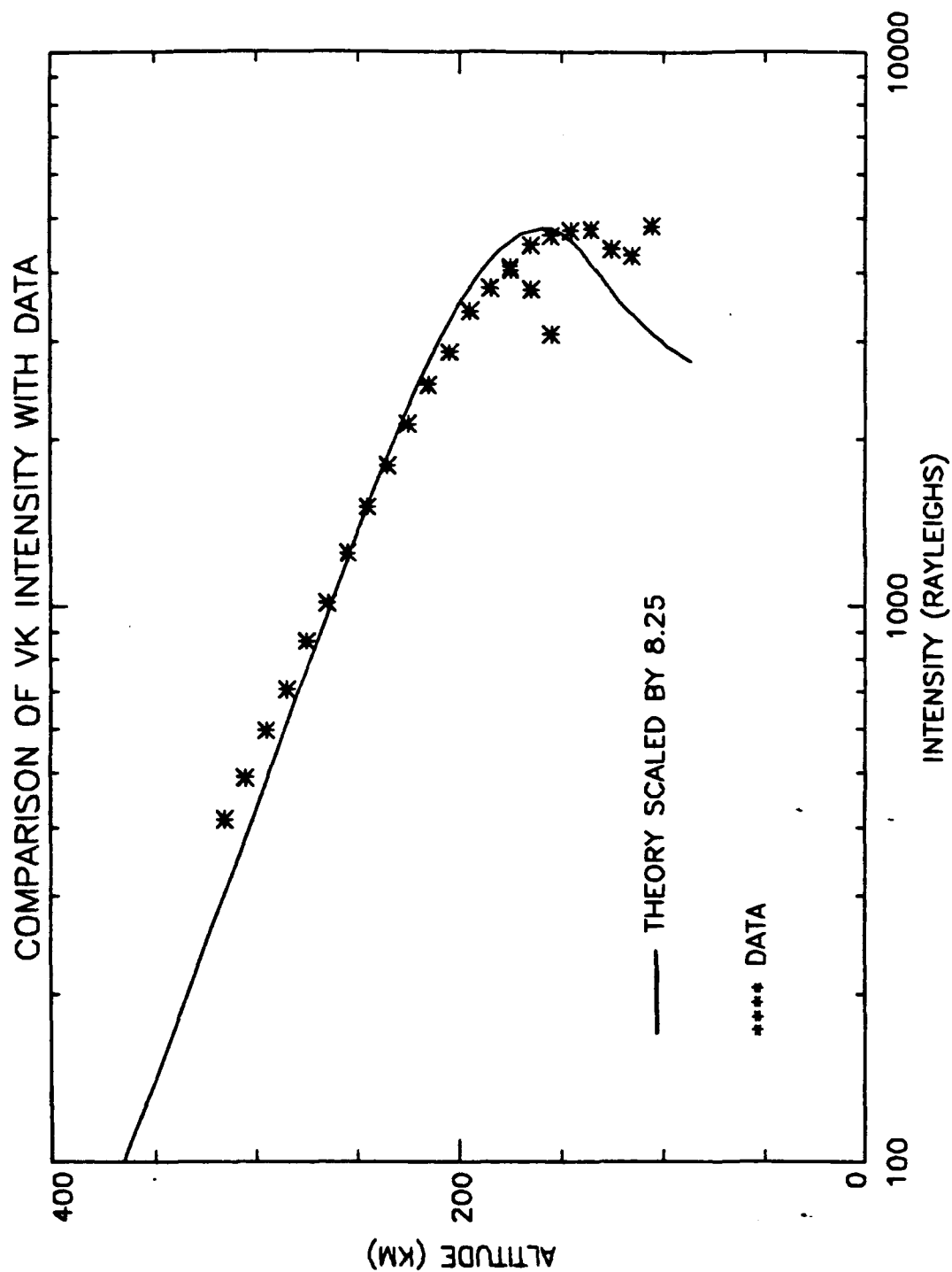


Figure 4-12 Comparison of the data with the model intensity profile for VK using MSIS values and changing the atomic oxygen quenching rate coefficient to  $q_0=9E-11$ .

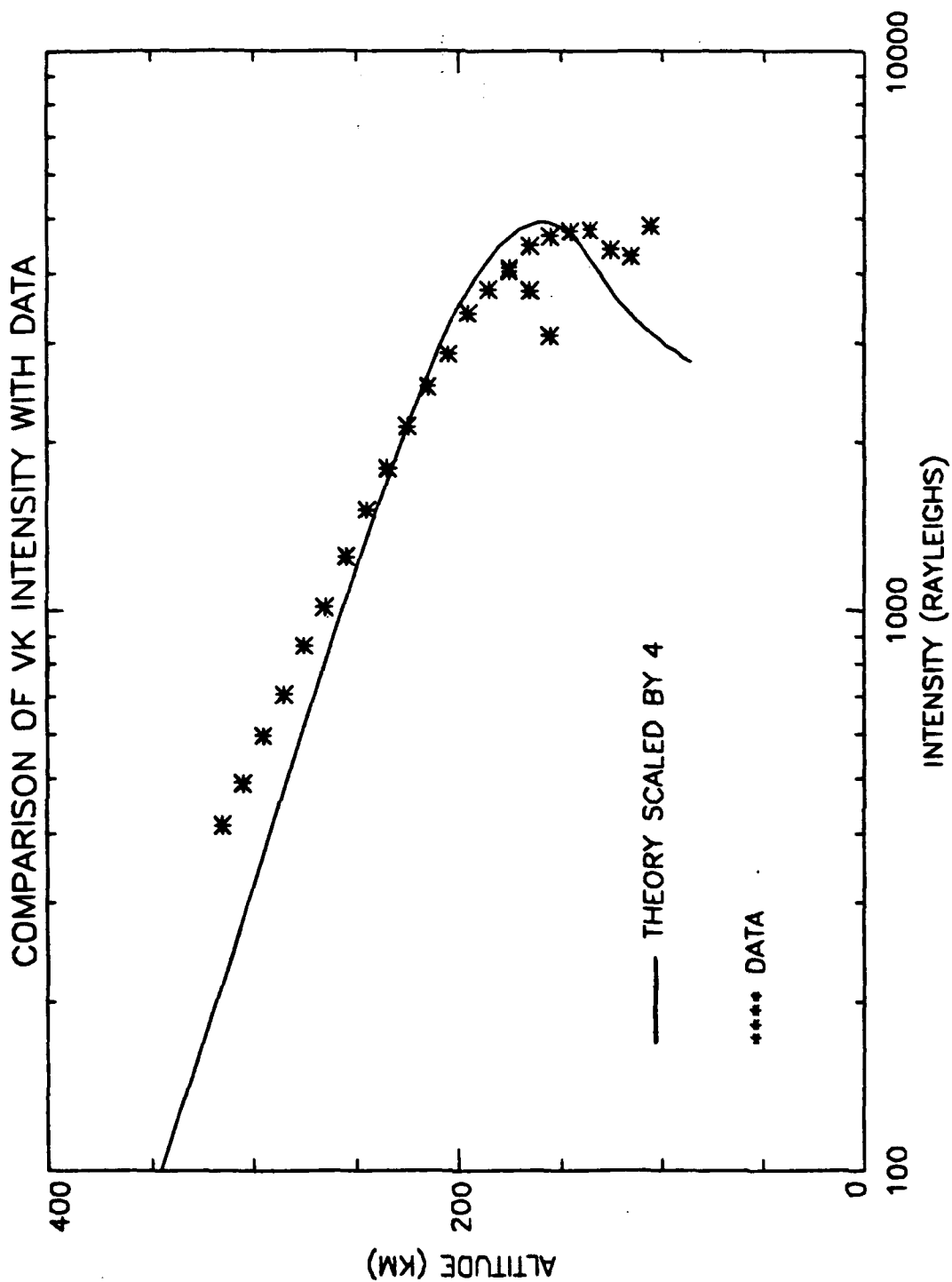


Figure 4-13 Comparison of the data with the model intensity profile for VK using MODATM values:  $T_{inf}=1600K$ ,  $-50\%$   $[O]_{120}$  and  $+30\%$   $[N]_{120}$ ; changing to  $q_i=9E-11$ .

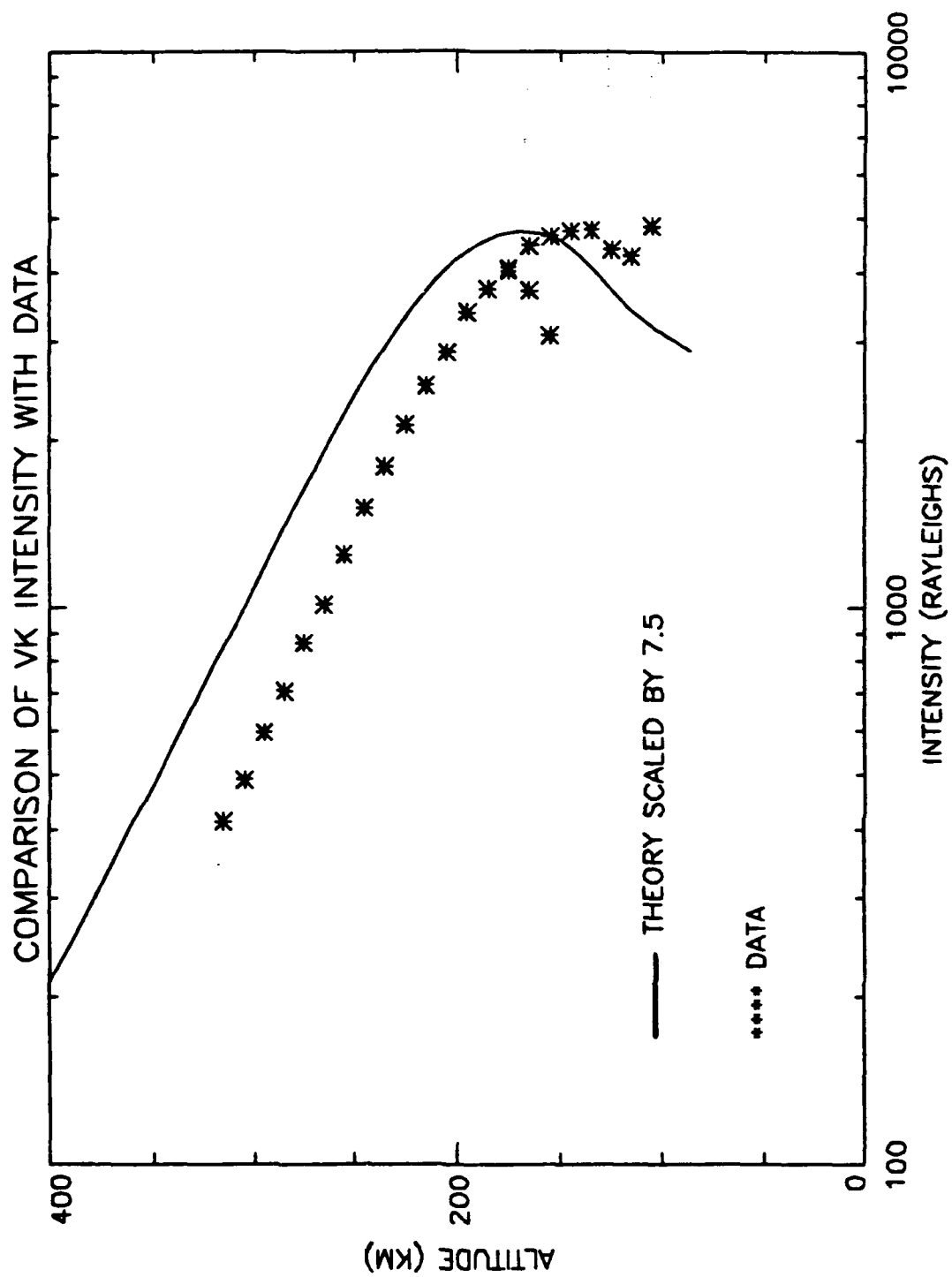


Figure 4-14 Comparison of the data with the model intensity profile for VK using MODATM value  $T_{inf}=1600$  and changing to  $q_c=9E-11$ .

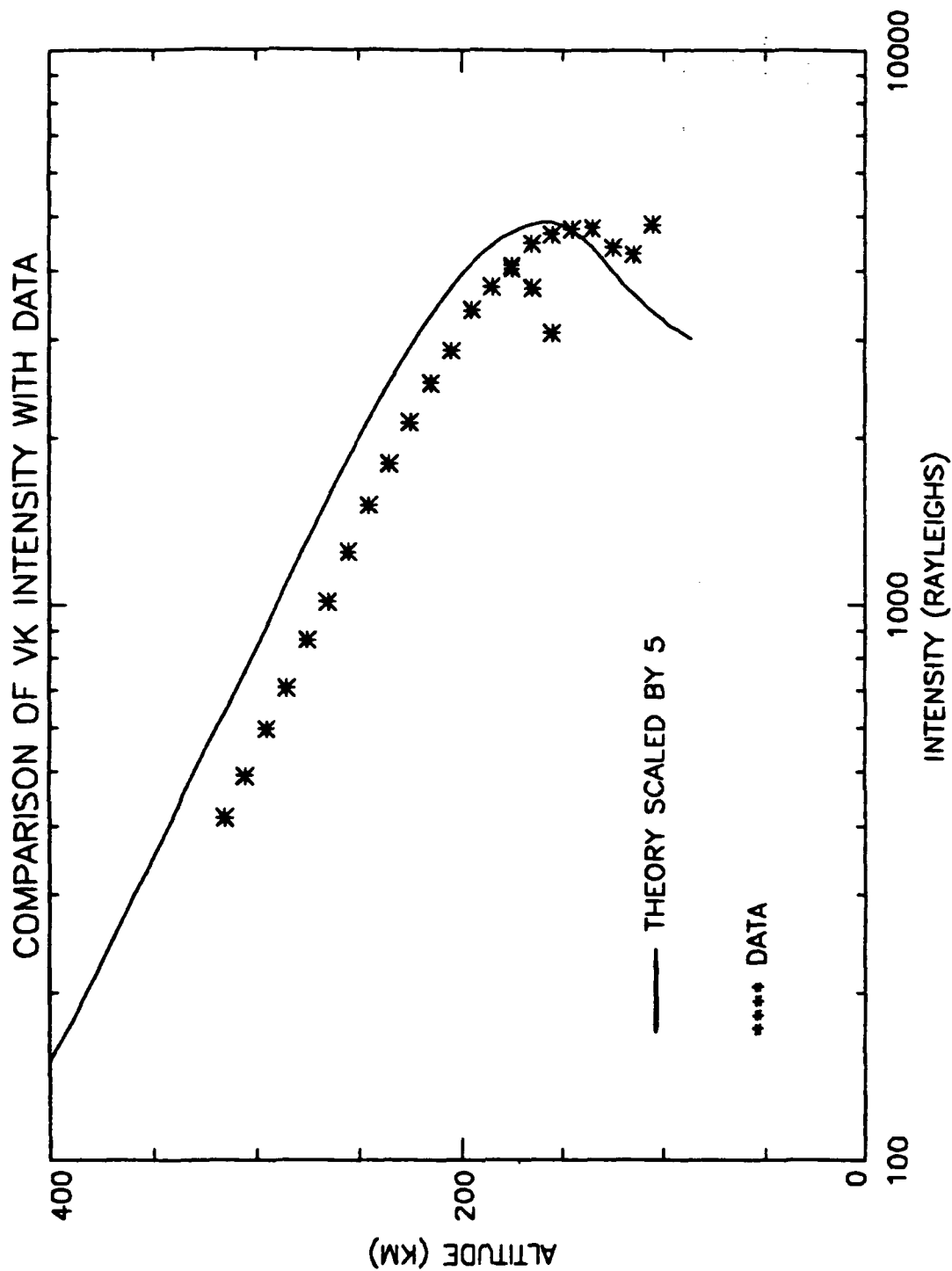


Figure 4-15 Comparison of the data with the model intensity profile for VK using MODATM value  $T_{inf}=1600K$  and changing to  $q_c=3E-11$ .

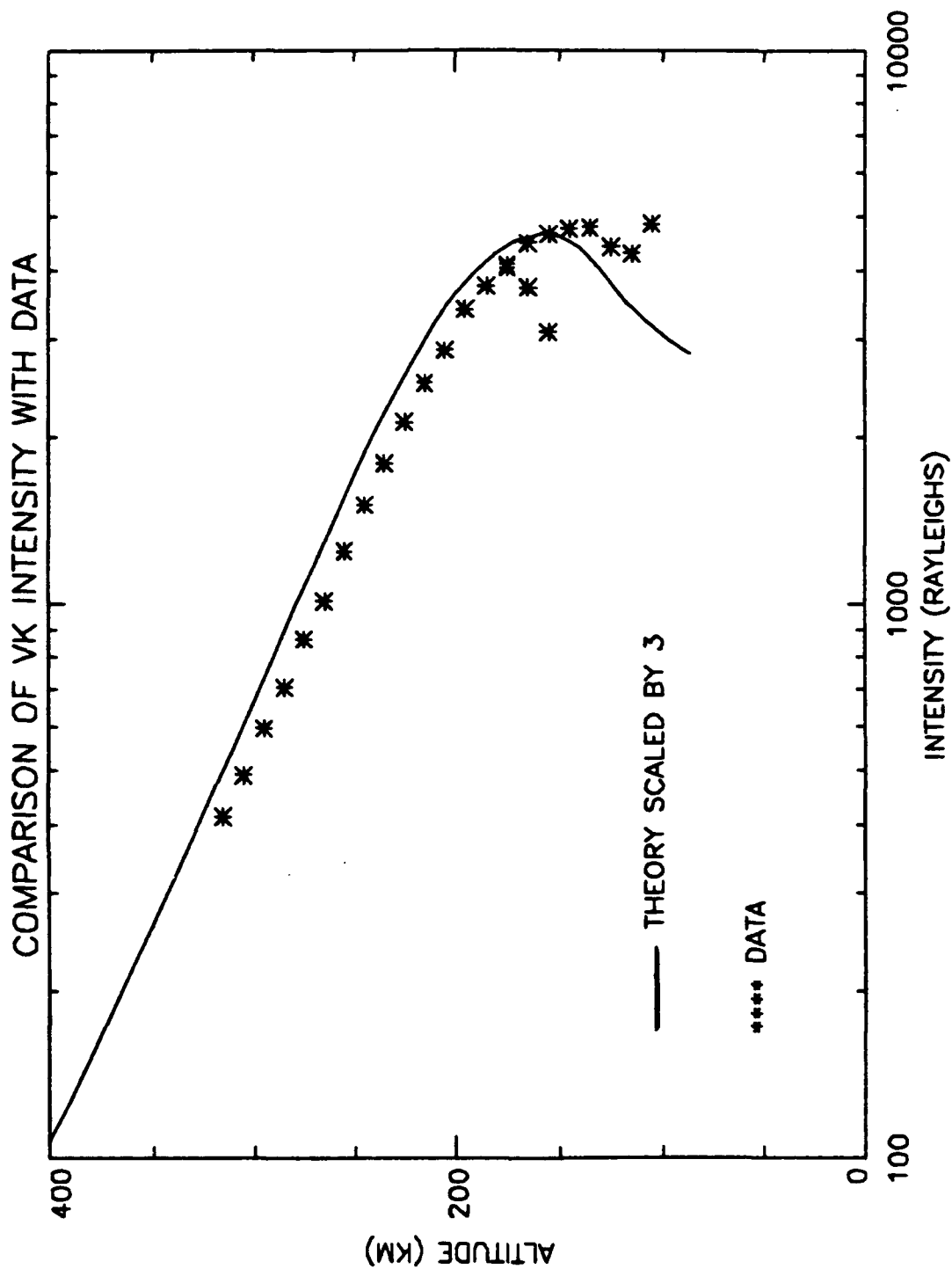


Figure 4-16 Comparison of the data with the model intensity profile for VK using MODATM values:  $T_{inf}=1600K$ ,  $-50\% [O]_{120}$ ,  $+30\% [N_2]_{120}$  and changing to  $q_i=3E-11$ .

(see Figure 4-17). This set of parameters was then used to fit the LBH data. This trial produced a good fit for the LBH only at the peak intensity and required scaling the prediction by 1.5 (see Figure 4-18). A good fit over the full range of the profile could not be achieved. Due to the nature of the log/linear plot, any difference between the curve and the data will be greatest at the peak. Therefore, the best fit was determined to be the one that best matched the peak. Additionally, the signal is the largest at the peak so the spectral analysis that produced the data points is most reliable there. The difference between the scaling factor required for the VK fit and the LBH fit is addressed below.

Previously, the analysis of VK was performed using an estimate for the branching ratio, denoted B00. A more accurate value for B00 was determined by taking the ratio of the relative number density at the zero vibrational quantum number to the total relative number density for the N2 excited state A. The new value for B00 was found to be 0.25 and Figure 4-19 shows the effect that this change has on the VK intensity profile. This curve required a scaling factor of 1.6 to achieve a good fit. This is consistent with the scaling factor of 1.5 required for LBH curve as shown in Figure 4-18.

The final emission used to analyze the data was the OI2972Å band. Using the model procedure OISLNT.PRO and

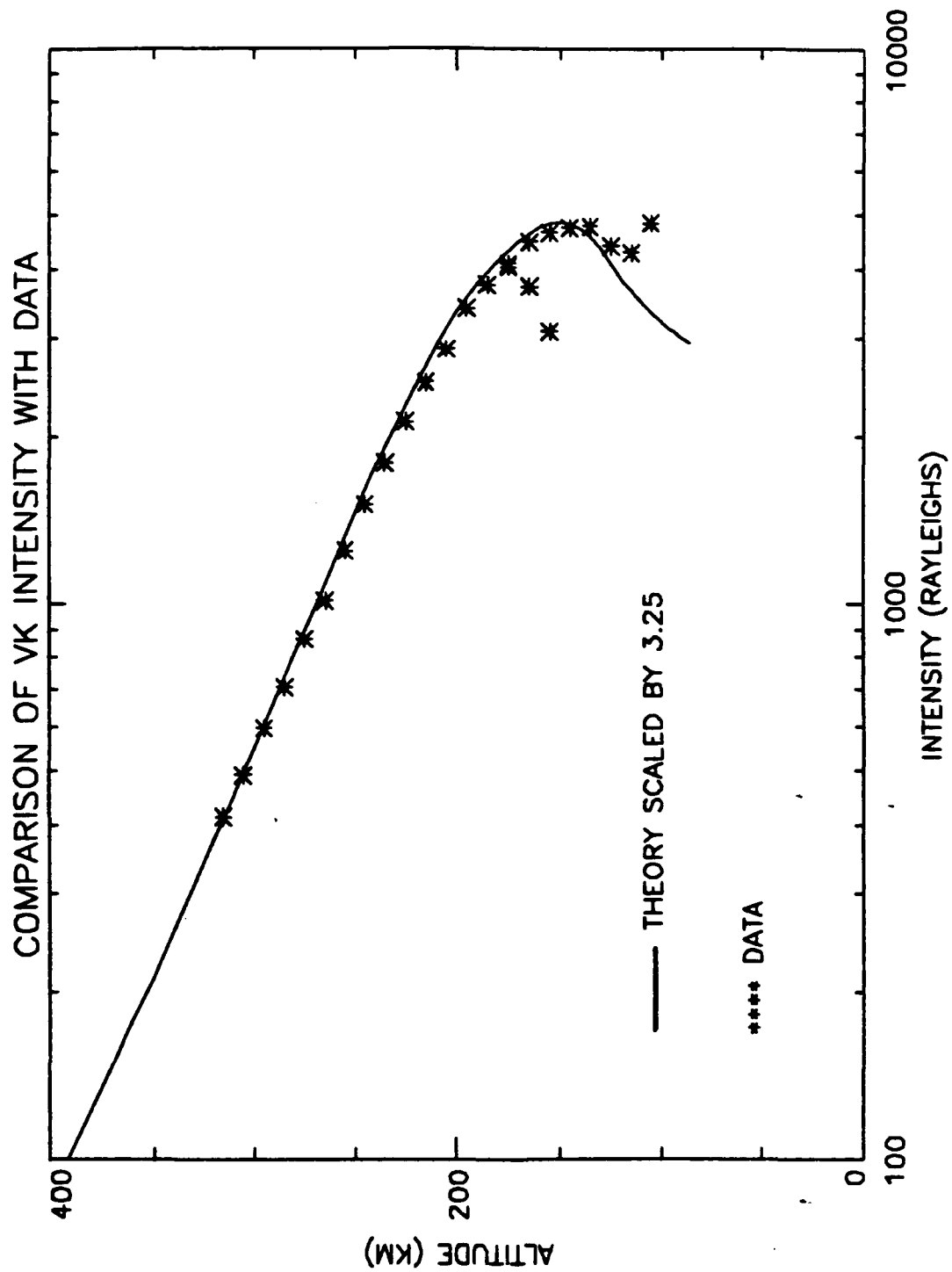


Figure 4-17 Comparison of the data with the model intensity profile for VK using MODATM values:  $T_{inf}=1600K$ ,  $-50\%$   $[O]_{120}$  and changing to  $q_c=3E-11$ .

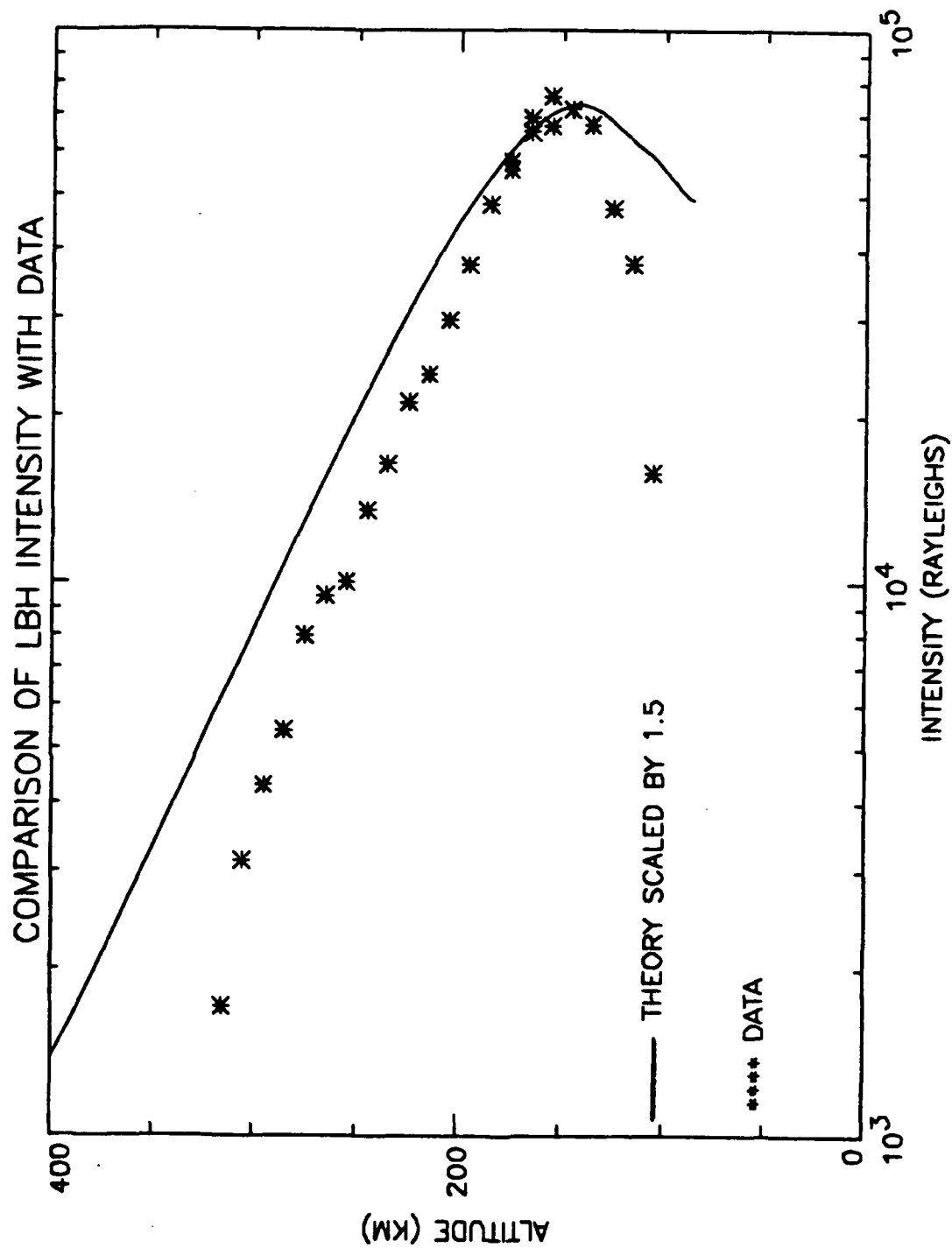


Figure 4-18 Comparison of the data with the model intensity profile for LBH using MODATM values:  $T_{inf}=1600K$  and  $-50\% [O]_{120}$ .



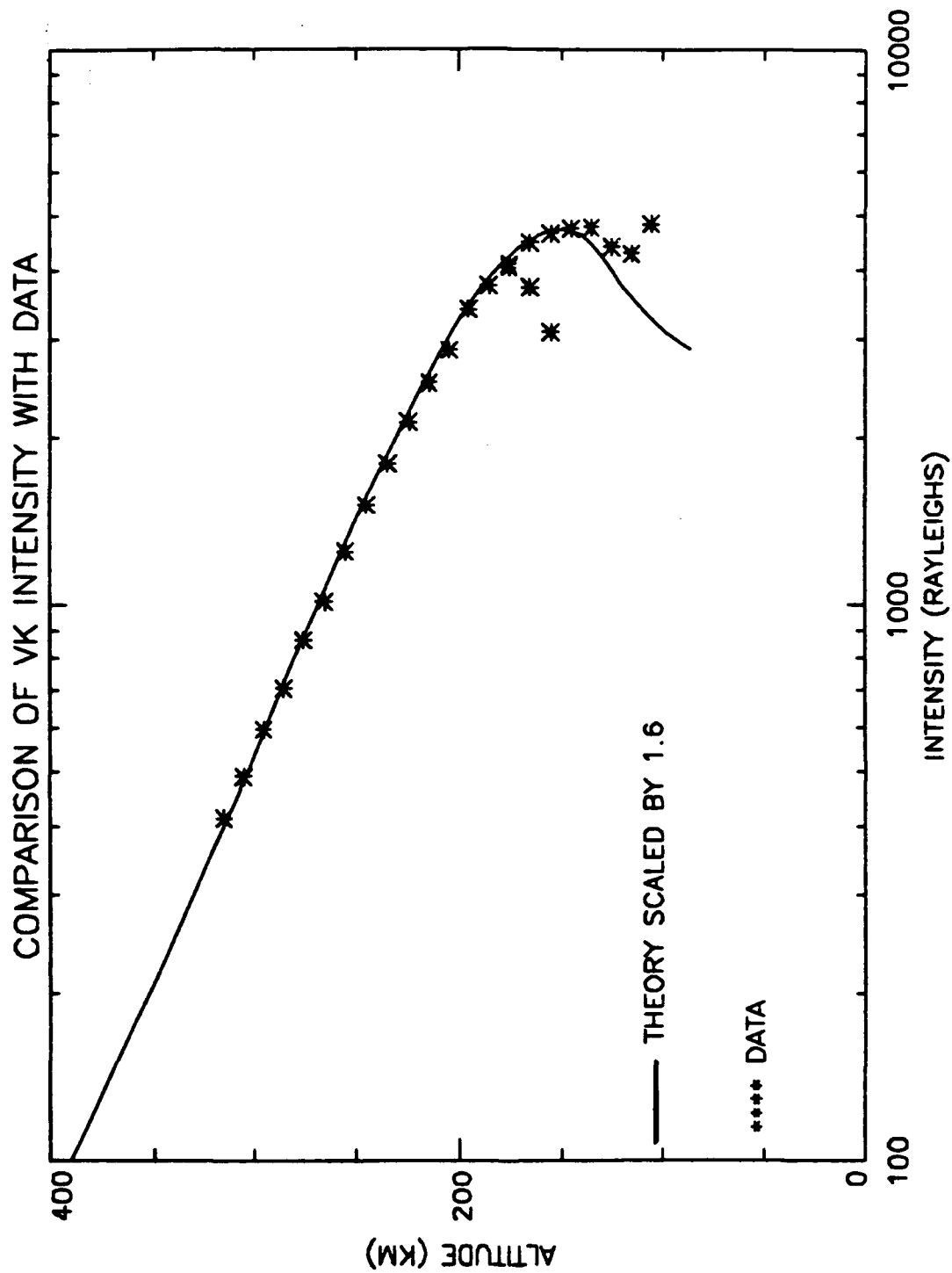


Figure 4-19 Comparison of the data with the model intensity profile for VK using MODATM values:  $T_{inf}=1600K$  and  $-50\%$   $[O]_{120}$ ;  $q_i=3E-11$  and changing to  $B00=0.25$ .

NEU6/FLX6, a predicted intensity profile was produced for this emission and compared with the data. As discussed in Chapter II, the profile calculated by OISLNT.PRO is only accurate for altitudes above 115 km. Because of this, only the upper altitudes were considered when attempting to fit the model profile to the data. A fair fit was achieved when the curve was scaled by 2.1. This is shown by the comparison of the model OI2972Å intensity profile with the data in Figure 4-20. Even though the analysis for the OI2972Å emission produced only a fair fit, it is important to remember that this is the least reliable band. Because a problem with the telemetry caused some data to be lost in the region of this wavelength (Walden, 1991), there is a systematic uncertainty in the 2972Å intensity profile. With the systematic error and the error inherent in the manual fitting technique, the 2.1 scaling factor is acceptable.

The above analysis indicated that the parameters from NEU6/FLX6 should correspond to the neutral atmosphere at the time of the launch. To test this, NOX1DIM.PRO (Cleary, 1986) was then run using these files and the profile for the electron density,  $[e^-]$ , was produced. This procedure uses the one dimensional MCE. A discussion of the results and a comparison of the calculated  $[e^-]$  profile with that of an ionosonde sounding performed by the Geophysics Laboratory (GL) at the time of the launch are presented in the following section. No comparison was made for the charged species

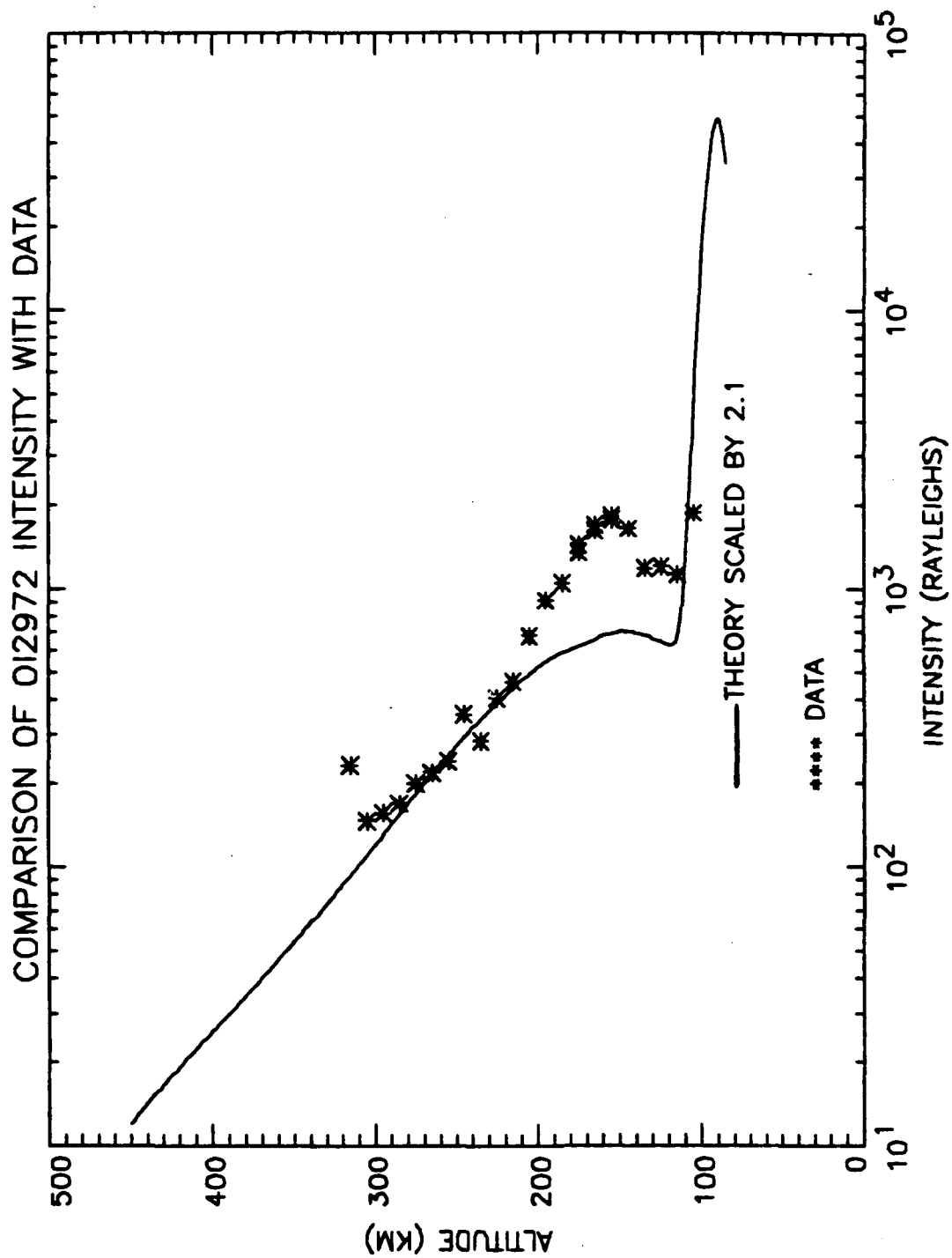


Figure 4-20 Comparison of the data with the model intensity profile for OI2972Å using MODATM values:  $T_{inf}=1600K$  and  $-50\%$  [O]<sub>120</sub>.

because no independent density profiles of these species exist for this launch.

In the course of writing this thesis, it was discovered that the W3D production rate was inadvertently omitted from the calculation for VK (see Equation 2-16). This omission caused a larger scaling factor to be required for all fits of VK. When the term was added, it was found that the best fit, NEU6/FLX6, fit without scaling. This is shown in Figure 4-21. Figures 4-22 and 4-23 shows two other figures for comparison to show that the ratio of the old scaling factor to the new scaling factor is approximately 1.6. This shows that the missing term was incorporated in the scaling factor. This applies only to VK and an approximate 1.5 scaling factor is still required for LBH and OI2972. This violates the requirement that the scaling factor for each emission be the same. If, for example, the scaling was accounting for a value for the solar flux which was too low, then the scaling factor would have to be the same for all emissions. The scaling factor is still important as an indicator of goodness of fit. Because the omission of the W3D term only resulted in a magnitude difference in all the VK plots, the above analysis would still have led to NEU6/FLX6 as the best fit.

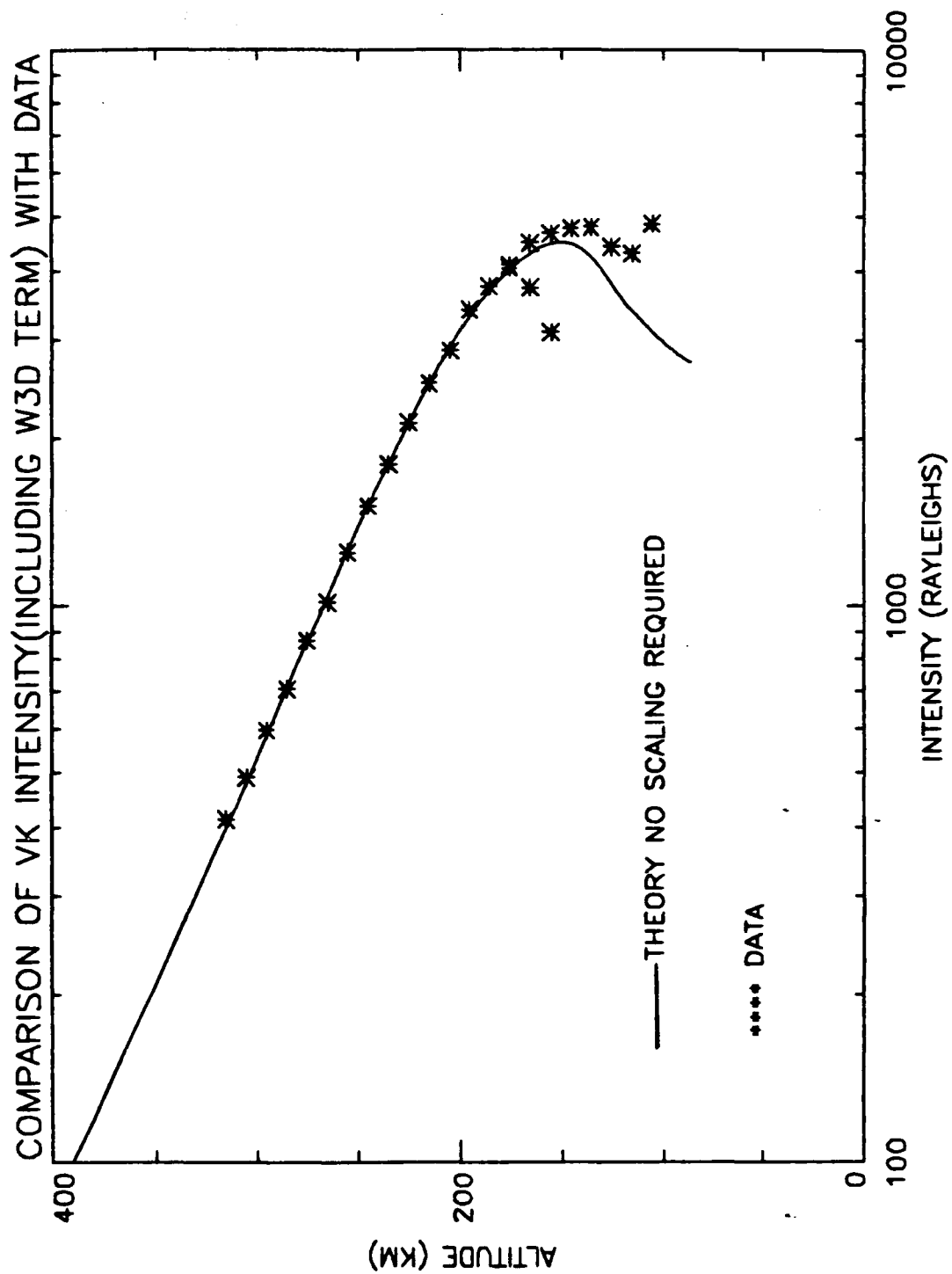


Figure 4-21  
production.

Re-plot of Figure 4-19 using correct VK

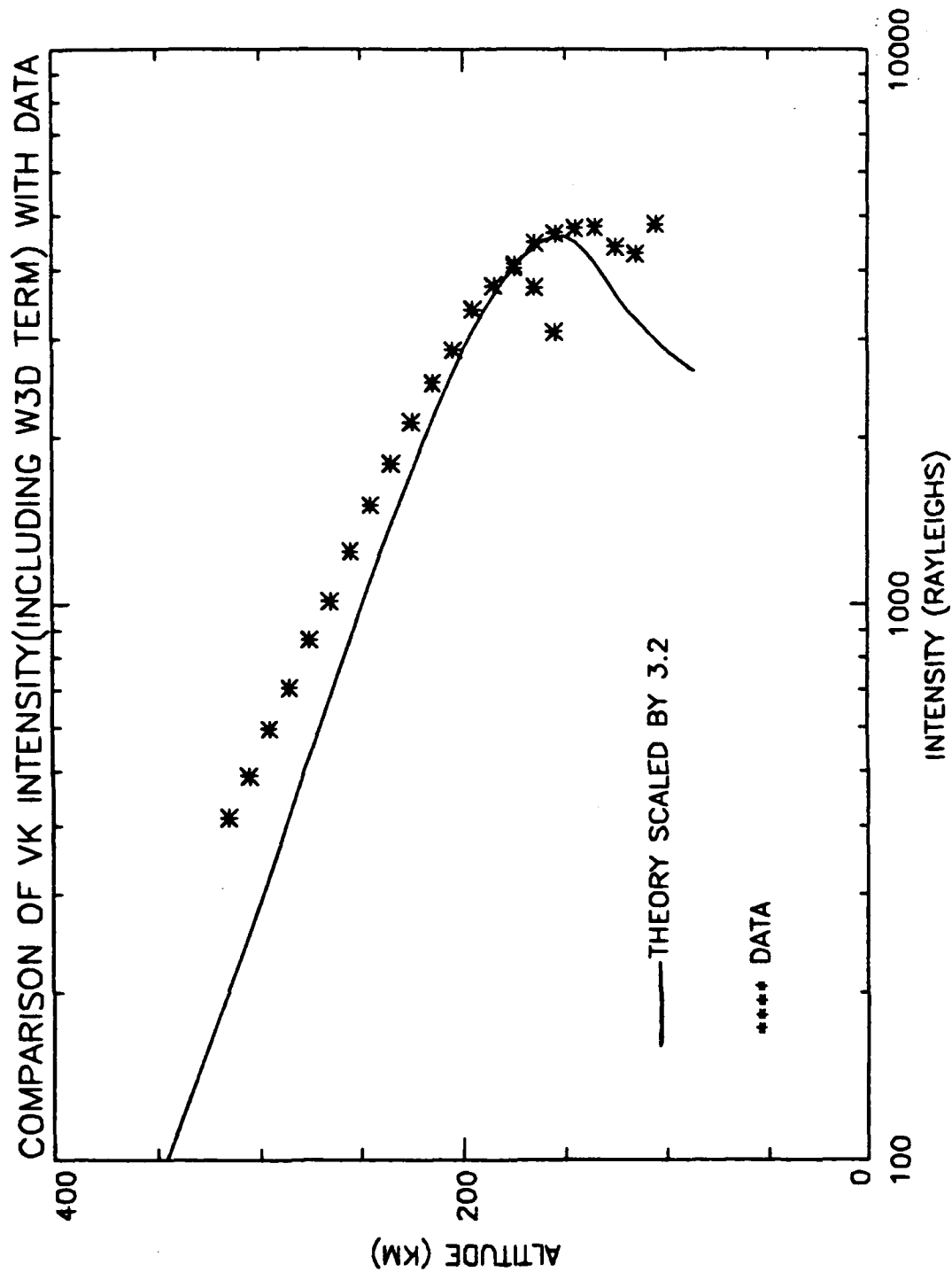


Figure 4-22  
production.

Re-plot of Figure 4-6 using correct VK

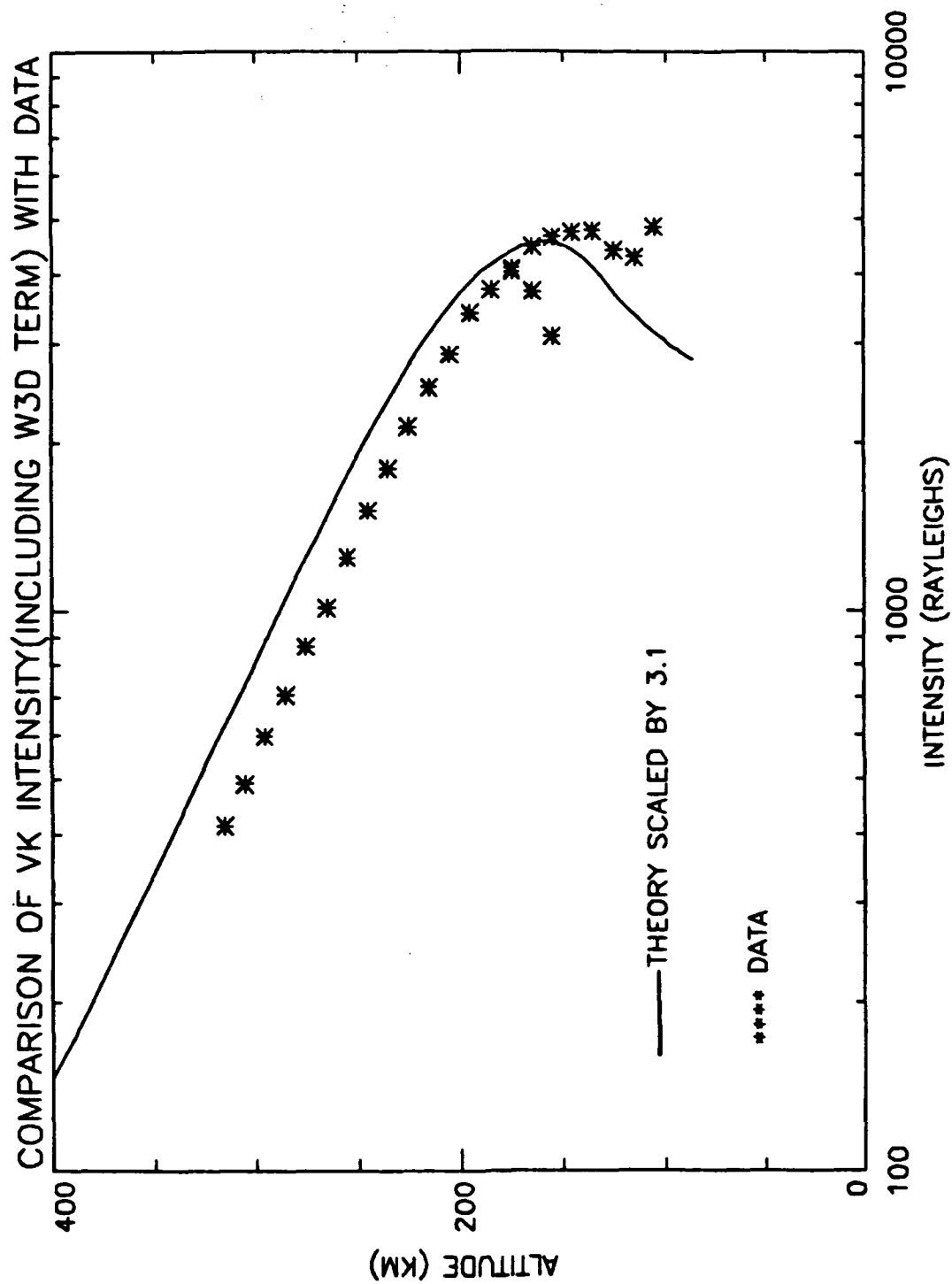


Figure 4-23  
production.

Re-plot of Figure 4-15 using correct VK

## B. RESULTS

The above analysis lead to an estimate of  $T_{inf}=1600K$  and a value for atomic oxygen density at 120 km of  $4.4E10\text{ cm}^{-3}$  which is half the MSIS3 calculated value. If NEU6 does in fact correspond to the neutral atmosphere at the time of the launch, then the  $[e^-]$  curve calculated by NOX1DIM using NEU6 would be expected to fit the  $[e^-]$  profile measured by GL. Figure 4-24 compares the NOX1DIM.PRO calculated  $[e^-]$  profile using NEU6 with the  $[e^-]$  profile from the GL ionosonde measurement (Bullett and Buchau, 1990). Figure 4-25 compares two NOX1DIM.PRO  $[e^-]$  calculations with the ionosonde data: one using the MSIS neutral atmosphere and the other using the NEU6 neutral atmosphere. This is intended to show whether any improvement can be seen in the calculated electron density profile by using the method describe above to determine the neutral atmosphere. As one can see, neither calculation agrees well with the GL data. The MSIS and the MODATM curves do seem to have the same general shape as the data from 90 to 160 km and 90 to 280 km respectively. The conclusions drawn from the above results follow in the next chapter.



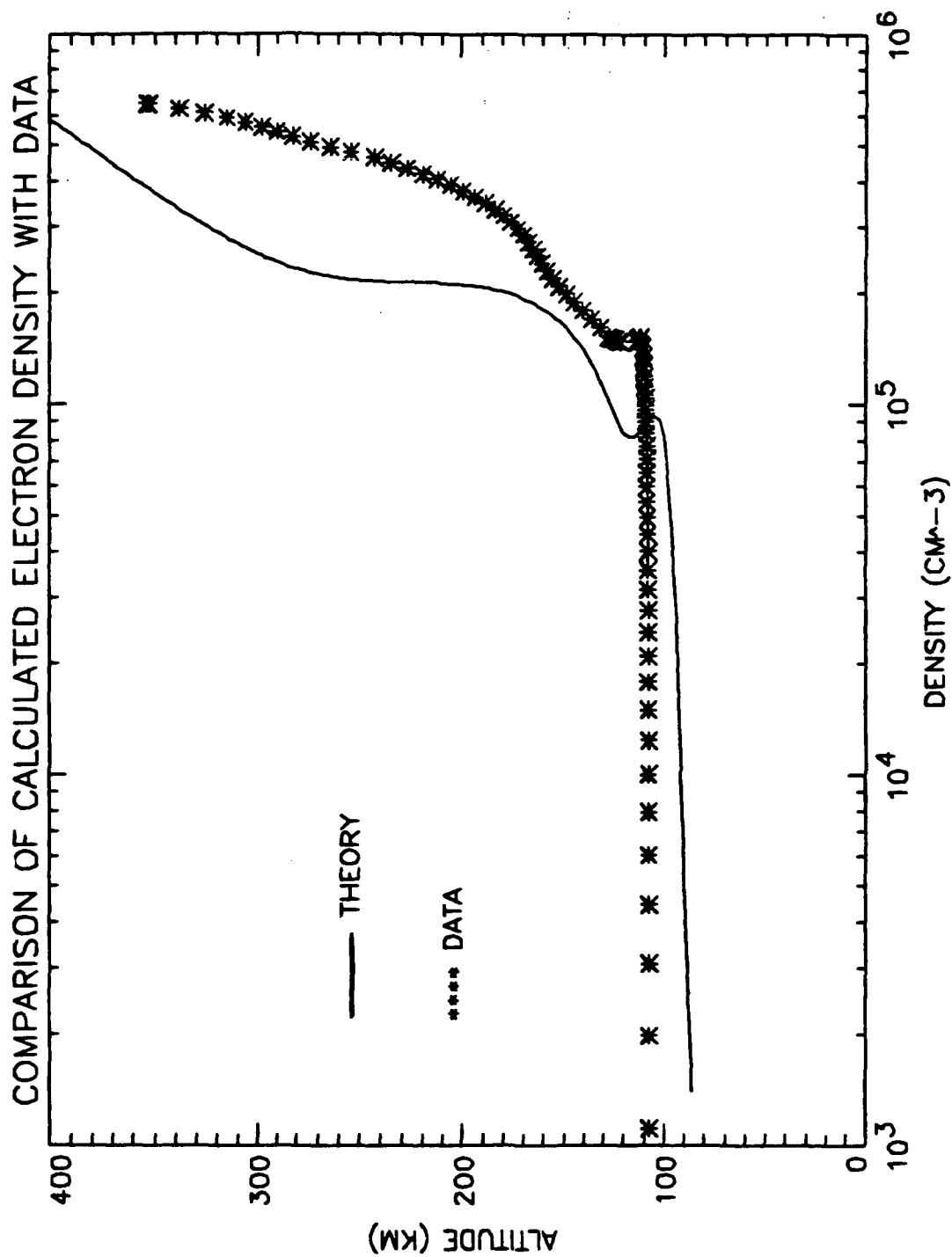


Figure 4-24 Comparison of the ionosonde data with the NOX1DIM calculated  $[e^-]$  profile using MODATM values:  $T_{inf}=1600K$  and  $-50\% [O]_{120}$ .

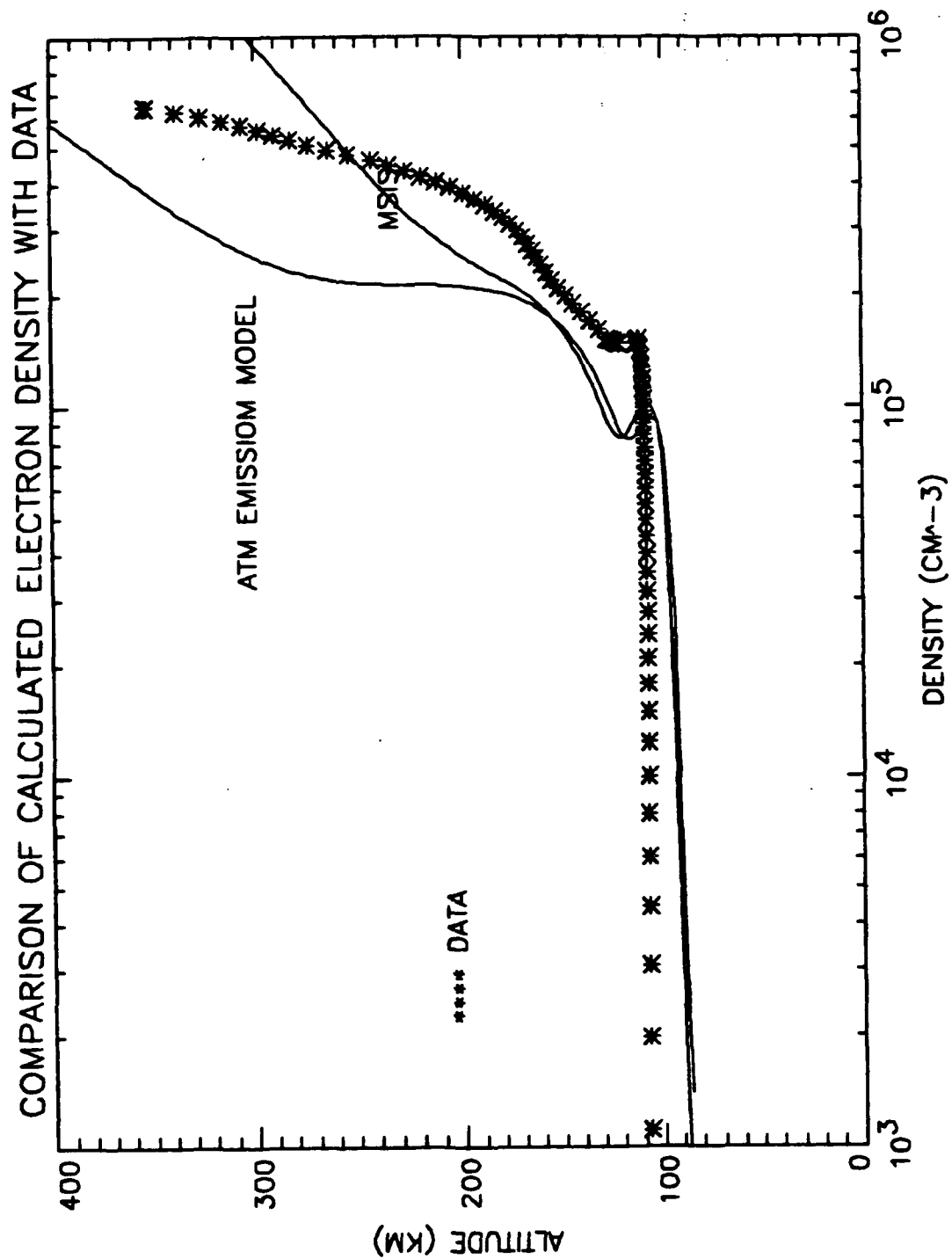


Figure 4-25 Comparison of the ionosonde data with the NOX1DIM calculated  $[e^-]$  profiles using MSIS values and using NEU6/FLX6 values.

## V. CONCLUSIONS

### A. SUMMARY

It was the aim of this thesis to develop a new technique for determining the densities of  $O$ ,  $O_2$  and  $N_2$  in the ionosphere. These species make-up the neutral atmosphere. It was hoped that by comparing calculated intensity profiles with the data, one could adjust the inputs until the model intensity profiles fit the data. The neutral atmosphere calculated by the model would then correspond to the neutral atmosphere at the time that the data was taken. This could then be used to determine the densities of the charged species and electrons.

The analysis method presented in this thesis did not, at first glance, appear to provide a viable approach for determining the neutral atmosphere or the densities of the charged species and electrons. This is somewhat misleading for several reasons. First, the data from the GL ionosonde measurement was taken 310 km north of the White Sands launch site. Normally, this would provide an accurate electron density profile for White Sands but at the time of the launch there was higher than normal geomagnetic activity. This resulted in a Traveling Ionospheric Disturbance or TID which distorted the ionosphere causing lower peak densities to occur at higher altitudes. These effects were reported by Bullett

and Buchau (1990) but could not be taken into account in the models used in the analysis. Also, since the ionosonde measurement was not taken in White Sands, the effects of the TID at the launch site could only be estimated and thus the  $[e^-]$  is also an estimate. Second, the experiment lost some data in the 2972Å wavelength region due to a problem with the telemetry circuit (Walden, 1991). Third, only the three emission bands were used. Using other prominent emissions would have helped the analysis. One emission that would have been particularly useful is the Second Positive band of molecular nitrogen. An analysis of this prominent band could not be performed because a synthetic spectrum model for the data currently does not exist. Another method for determining the intensity profile for the Second Positive suggested by Walden (1991) proved to be unworkable. Had the OI2972Å emission been more reliable and if the Second Positive band had been available, a better calculation might have been possible using the above analysis method. Finally, the scaling factor of approximately 1.6 which was necessary to achieve a good fit for LBH and OI2972Å is not understood. It suggests that there is uncertainty in the models for the LBH and OI2972Å emissions. The excellent fit of VK also suggests that the data for both LBH and OI2972Å is less reliable than originally believed. One last conclusion that can be drawn from this thesis is that the excellent fit for VK and LBH (once scaled) in scale height indicates a  $T_{inf}=1600K$  which is

higher than the  $T_{inf}$  calculated by the MSIS3 model. It also is different than the 1500K and 1700K suggested by Mack (1991). The  $T_{inf}=1600K$  resulted in much better scale height agreement for the intensity curves.

The method described in this thesis did not produce a neutral atmosphere which led to an electron density profile that fit the Geophysics Laboratory data. Although this is true, this approach cannot be dismissed. Improving the problem areas discussed above should allow this method to successfully calculate the neutral atmosphere as well as the charged species and electron density curves.

#### B. SUGGESTIONS FOR FOLLOW-ON RESEARCH

As pointed out in the summary section, there are several areas in which improvements can be made to better test the viability of this method for analyzing the ionosphere. First, improvements were made for the 1992 launch which should have increased the accuracy of the data collected. One such improvement was better telemetry electronics which eliminated the data drop problems that hurt the information collection in 1990. Using this better data, the synthetic spectrum fitting performed by Walden (1991) should be repeated to get the intensity profiles for VK, LBH and OI2972Å. The elimination of the drops in the data should result in a more accurate intensity profile for OI2972Å. Additionally, the model for OI2972Å should be extended to include the lower altitude

profile of this emission. Second, a synthetic spectrum should be developed for the Second Positive band. As was suggested by Walden (1991), the known contributions of  $N_2$  could be subtracted from the data and the remainder could be assumed to be the Second Positive spectrum. This should now be practical with the better 1992 launch data. Third, other emissions should also be used in the fit process. Using several emissions should lead to better results. Fourth, the scaling requirement should be more fully investigated. Possible refinements in the models for LBH and OI2972 as well as the better data for the 1992 launch should be able to eliminate these. Lastly, an effort should be made to fully integrate the atmospheric emission model, the MSIS3 model, MODATM, and NOX1DIM into a single program that uses numerical methods to automatically determine the fit. This would be necessary to make this method practical for analyzing the large amount of data received from a satellite-based spectrograph. If the above changes are implemented, this method and the data from satellites could be used to make timely ionospheric profile calculations possible for any point on the globe.

## APPENDIX

The Appendix contains the IDL code for the Atmospheric Emission Model.

```
;THIS PROCEDURE GETS THE O,O2,N2  
;DENSITIES  
;AND CORRESPONDING ALT FROM EITHER  
;MSIS.DAT OR NEU'V'.DAT  
;FILES FOR USE IN GETVE.PRO.  
;WRITTEN BY KENNETH L. MCELROY  
;15 MAY 1992
```

```
PRO GETDENS,OALT,ODEN,O2DEN,N2DEN,TEMP  
FILE=' '  
READ,'WHAT DATA FILE DO YOU WANT TO USE?(I.E. 90089MSIS.DAT OR 90089NEU"V".DAT)'  
,FILE  
OPENR,2,FILE  
B=ASSOC(2,FLTARR(183))  
OALT=B(1)  
TEMP=B(2)  
ODEN=B(3)  
O2DEN=B(4)  
N2DEN=B(5)  
CLOSE,2  
RETURN  
END
```

```

;THIS PROG READS THE ALT AND VOL
;PROD RATES A1P,A3S,B3P,C3P, AND W3D
;FOR N2 FROM FLX'V'.PRT OR
;FLXM.PRT FILES
;WRITTEN BY K.L. MCELROY
;23 APR 1992
;MODIFIED 06 JUNE 92

PRO GETXRATE,ALT,A1P,A3S,B3P,C3P,W3D,OI
  file=' '
  read,'What file do you want to use?(FLX"V".PRT OR FLXM.PRT)',file
  OPENR,1,FILE

;THIS SECTION GETS ALT AND A3S
;FOR N2

STR1=' '
WHILE STRPOS(STR1,'VOLUME PRODUCTION RATES') EQ -1 DO READF,1,STR1
FOR J=1,5 DO READF,1,STR1
ALT=FLTARR(51)
A3S=FLTARR(51)
R1=FLTARR(11)
FOR J=0,50 DO BEGIN
  READF,1,R1
  ALT(J)=R1(0)
  A3S(J)=R1(10)
ENDFOR

;THIS SECTION GETS A1P,B3P,C3P
;AND W3D

STR2=' '
FOR J=1,7 DO READF,1,STR2
A1P=FLTARR(51)
B3P=FLTARR(51)
C3P=FLTARR(51)
W3D=FLTARR(51)
R2=FLTARR(5)
FOR J=0,50 DO BEGIN
  READF,1,R2
  A1P(J)=R2(4)
  B3P(J)=R2(1)
  C3P(J)=R2(2)
  W3D(J)=R2(3)
ENDFOR
WHILE STRPOS(STR2,'OI') EQ -1 DO READF,1,STR2
FOR J=1,3 DO READF,1,STR2
OI=FLTARR(51)
FOR J=0,50 DO BEGIN
  READF,1,R2
  OI(J)=R2(3)
ENDFOR
CLOSE,1
RETURN
END

```



```

;THIS PROCEDURE USES GETXRATE.PRO AND
;GETODEN.PRO TO GET VOLUME EXCITATION RATES
;FOR VK, LBH, AND SECPOS FOR SLNTINT.PRO
;WRITTEN BY K.L. MCELROY
;15 MAY 1992
;MODIFIED:14 SEP 92

PRO GETVE,ALT,VVK,VLBH,VSECPOS,DENOM
GETXRATE,ALT,A1P,A3S,B3P,C3P,W3D
GETDENS,OALT,ODEN
A=.5
B00=.125
QO=3E-11
QO5=1.69E-1
O=INTERPOL(ODEN,OALT,ALT)
VLBH=A1P
VSECPOS=C3P/2.
DENOM=(1.+QO*O/A)
VVK=((A3S+B3P+C3P/2.)*B00*QO5)/DENOM
RETURN
END
@GETXRATE
@GETDENS

```

```

;THIS IS 1/LIFETIME OF A STATE(S^-1)
;THIS THE BRANCHING RATIO
;THIS IS O QUENCHING COEFF.(CM^3 S^-1)
;THIS IS THE FRANK-CONDON FACTOR FOR 0-5

```

```

;THIS PROCEDURE CONVERTS VOL EX RATES
;FROM GETVE.PRO TO SLANT INTENSITIES
;FOR VK, LBH, AND SECPOS OF N2
;WRITTEN BY K.L.MCELROY
;23 APR 1992
;MODIFIED: 15 MAY 92

```

```

pro slntint,att0,alt,svk,slbh,ssecpos,denom
getve,alt,vvk,vlbh,vsecpos,denom
att=alt*0+att0
delalt=alt(0)-alt(5)
tophvk=abs(delalt/alog(vvk(5)/vvk(0)))
topvevk=vvk(0)*exp(-2./tophvk)
tophlbh=abs(delalt/alog(vlbh(5)/vlbh(0)))
topvelbh=vlbh(0)*exp(-2./tophlbh)
tophc3pi=abs(delalt/alog(vsecpos(5)/vsecpos(0)))
topvec3pi=vsecpos(0)*exp(-2./tophc3pi)
volslnt,vvk,alt,att,topvevk,tophvk,svk
volslnt,vlbh,alt,att,topvelbh,tophlbh,slbh
volslnt,vsecpos,alt,att,topvec3pi,tophc3pi,ssecpos
svk=svk*1e-6
slbh=slbh*1e-6
ssecpos=ssecpos*1e-6
return
end
@getve

```

```
;THIS PROCEDURE CALCULATES THE SLANT
;INTENSITIES FOR OI(2972).
;WRITTEN BY K.L. MCELROY
;11 JULY 1992
;MODIFIED: 16 SEP 92
```

```
PRO OISLNT,ATT0,ALT183,SOI
ATT=FLTARR(183)
ATT=ATT*0+ATT0
A2972=0.045
A5577=1.06
B=.1
K2=2.1E-8
K3=5E-11
V=' '
```

```
;THESE ARE THE EINSTEIN COEFFICIENTS
;THIS IS THE BRANCHING RATIO
```

```
READ,'WHAT VERSION OF FILES DO YOU WANT?',V
```

```
;THIS SECTION GETS THE FIRST
;PRODUCTION FACTOR P1
```

```
OPENR,1,'90089FLX'+V+'.PRT'
STR1=' '
WHILE STRPOS(STR1,'VOLUME PRODUCTION RATE') EQ -1 DO READF,1,STR1
WHILE STRPOS(STR1,'SPECIES OI') EQ -1 DO READF,1,STR1
FOR J=1,3 DO READF,1,STR1
ALT=FLTARR(51)
OIS=FLTARR(51)
R1=FLTARR(11)
FOR J=0,50 DO BEGIN
  READF,1,R1
  ALT(J)=R1(0)
  OIS(J)=R1(3)
ENDFOR
CLOSE,1
```

```
;THIS SECTION GETS THE
;DENSITIES FOR O2+ & ELEC
```

```
OPENR,1,'90089ION'+V+'.DAT'
A=ASSOC(1,FLTARR(183))
O2P=FLTARR(183)
ELEC=FLTARR(183)
O2P=REVERSE(A(5))
ELEC=REVERSE(A(6))
CLOSE,1
```

```
;MAKES O2P AND ELEC ARRAYS GO
;FROM HIGH TO LOW
```

```
OPENR,1,'90089NOX'+V+'.DAT'
A=ASSOC(1,FLTARR(183))
N4S=FLTARR(183)
N4S=REVERSE(A(1))
CLOSE,1
```

```
;THIS SECTION GETS N4S DENSITY
```

```
;MAKES ARRAY GO FROM HIGH TO LOW
```

```
;THIS CONVERTS OIS FROM
;A FLTARR(51) TO FLTARR(183)
```

```

ALT183=FINDGEN(183)*2.+86
ALT183=REVERSE(ALT183)
O1SDEN=INTERPOL(O1S,ALT,ALT183)

```

```

GETDENS, OALT, ODEN, O2DEN, N2DEN, TEMP
ODEN=REVERSE(ODEN)
O2DEN=REVERSE(O2DEN)
N2DEN=REVERSE(N2DEN)
M=ODEN+O2DEN+N2DEN

```

```

T=REVERSE(TEMP)
K4=4.7E-33*(300/T)^2

```

```

P1=O1SDEN
P2=K2*B*O2P*ELEC
P3=K3*O2P*N4S
P4=K4*ODEN^2*M
L=A2972+A5577
VOI=(P1+P2+P3+P4)/L*A2972

```

```

DELALT=ALT183(0)-ALT183(5)
TOPHOI=ABS(DELALT/ALOG(VOI(5)/VOI(0)))
TOPVEOI=VOI(0)*EXP(-2./TOPHOI)
VOLSLNT, VOI, ALT183, ATT, TOPVEOI, TOPHOI, SOI

```

```

SOI=SOI*1E-6
RETURN
END
@GETDENS

```

```

;THIS SECTION GETS O, O2 & N2
;DENSITIES AND TEMP NEEDED FOR
;P4

```

```

;THESE COMMANDS MAKE THE
;DENSITIES GO FROM HIGH TO LOW

```

```

;MAKES TEMP GO FROM HIGH TO LOW

```

```

;THIS SECTION CALCULATES THE VE
;FOR OI2972

```

```

;THIS SECTION CALCULATES THE
;SLANT INTENSITY FOR OI2972

```

```

;THIS CONVERTS TO RAYLEIGHS

```

## LIST OF REFERENCES

Bullett, Terence and Buchau, Jurgen, "Ionospheric Electron Density Profiles over White Sands Missile Testing Range on 30 March 1990," Report by Ionospheric Effects Branch, Ionospheric Physics Division, Geophysics Laboratory (AFSC), 05 November 1990.

Cartwright, David C., "Vibrational Populations of the Excited States of  $N_2$  Under Auroral Conditions," J. Geophys. Res., 83, No. A2, 517, 01 February 1978.

Cleary, David D., Analysis of Nitric Oxide Fluorescence Bands from High Latitude Rocket Observations of the Thermospheric Dayglow, Ph.D. Dissertation, University of Colorado, 1985.

Cleary, D.D., "Daytime High-Latitude Rocket Observations of the NO  $\gamma, \delta$ , and  $\epsilon$  Bands," J. Geophys. Res., v. 91, 1986.

De Souza, A.R., Gousset, G., Touzeau, M., and Tu Khiet, "Note on the Determination of the Efficiency of the Reaction  $N_2(A^3\Sigma) + O(^3P) \rightarrow N_2 + O(^1S)$ ," J. Phys. B18, L661, 1985.

Hedin, A.E., A Revised Thermospheric Model Based on Mass Spectrometer and Incoherent Scatter Data: MSIS-83, J. Geophys. Res., 88, 10170, 1983.

Mack, Bryan D., An Analysis of Middle Ultraviolet Emissions of Molecular Nitrogen and Nitric Oxide and Vacuum Calibration of an Ultraviolet Spectrograph, Master's Thesis, Naval Postgraduate School, Monterey, California, June 1991.

Meier, R.R., "Ultraviolet Spectroscopy and Remote Sensing of the Upper Atmosphere," Space Science Reviews, v. 58, nos. 1 & 2, October 1991.

Piper, G.L. and Caledonia, G.E., "Rate Constants for Deactivation of  $N_2(A^3\Sigma_u^-)$ ,  $v' = 0, 1$  by O," J. Chem. Phys. 75, 2847, 1981.

Private conversation between D. Cleary, Naval Postgraduate School, and the author, 01 April 1992.

Quint, John H., Development of an NPS Middle Ultraviolet Spectrograph (MUSTANG) Electronic Interface Package, Master's Thesis, Naval Postgraduate School, Monterey, California, December 1991.

Sharp, W.E., "Rocket-borne Spectroscopic Measurements in the Ultraviolet Aurora: Nitrogen Vegard-Kaplan Bands," J. Geophys. Res., 76, 987, 1971.

Strickland, D.J., and R.R. Meier, A Photoelectron Model for the Rapid Computation of Atmospheric Excitation Rates, NRL Memorandum Report, 5004, 1982.

Thomas, J.M. and Kaufman, F., "Rate Constants of the Reactions of Metastable  $N_2(A^3\Sigma_u^-)$  in  $v = 0, 1, 2$ , and 3 with Ground State  $O_2$  and O," J. Chem. Phys. 83, 2900, 1985.

Torr, Marsha R. and Torr, D.G., "The Role of Metastable Species in the Thermosphere," J. Geophys. Res., 20, pp. 91-144, February 1982.

Walden, Billie S., An Analysis of Middle Ultraviolet Dayglow Spectra, Master's Thesis, Naval Postgraduate School, Monterey, California, December 1991.

# INITIAL DISTRIBUTION LIST

1. Defense Technical Information Center 2  
Cameron Station  
Alexandria, Virginia 22304-6145
2. Library, Code 052 2  
Naval Postgraduate School  
Monterey, California 93943-5002
3. Dr. K.E. Woehler, Chairman PH 1  
Physics Department  
Naval Postgraduate School  
Monterey, California 93943-5000
4. Dr. D.D. Cleary 3  
Physics Department, PH-C1  
Naval Postgraduate School  
Monterey, California 93943-5002
5. Dr. S. Gnanalingam 1  
Physics Department, PH-Gm  
Naval Postgraduate School  
Monterey, California 93943-5002
6. LT Kenneth L. McElroy Jr. 4  
c/o Mrs. Faye T. McElroy  
728 W. Ivy Dr.  
Seaford, Delaware 19973
7. Mr. and Mrs. James R. Stewart 1  
1896 W. Chestnut  
Exeter, California 93221